AGU PUBLICATIONS

JGR

Journal of Geophysical Research: Oceans

RESEARCH ARTICLE
10.1002/2013JC009603

Special Section:
Pacific-Asian Marginal Seas

ITCZ and ENSO pacing on East Asian winter monsoon variation during the Holocene: Sedimentological evidence from the Okinawa Trough

Xufeng Zheng[1,2], Anchun Li[1], Shiming Wan[1], Fuqing Jiang[1], Shuh Ji Kao[3], and Cody Johnson[4]

[1]Key Laboratory of Marine Geology and Environment, Institute of Oceanology, Chinese Academy of Sciences, Qingdao, China, [2]Key Laboratory of Marginal Sea Geology, South China Sea Institute of Oceanology, Chinese Academy of Sciences, Guangzhou, China, [3]State Key Laboratory of Marine Environmental Science, Xiamen University, Xiamen, China, [4]Department of Civil and Environmental Engineering, Louisiana State University, USA

Key Points:
- The newly proposed grain-size index reveals various transport mechanisms
- The intensity of East Asian winter monsoon was modulated by the ITCZ
- An intensified ENSO since 5 kyr weakens EAWM and EASM relationship

Correspondence to:
A. Li,
acli@ qdio.ac.cn

Citation:
Zheng, X., A. Li, S. Wan, F. Jiang, S. J. Kao, and C. Johnson (2014), ITCZ and ENSO pacing on East Asian winter monsoon variation during the Holocene: Sedimentological evidence from the Okinawa Trough, *J. Geophys. Res. Oceans*, *119*, 4410–4429, doi:10.1002/2013JC009603.

Received 15 NOV 2013
Accepted 24 JUN 2014
Accepted article online 27 JUN 2014
Published online 21 JUL 2014

Abstract Deep-sea fan sediments provide an excellent geological archive for paleoenvironment reconstruction. Grain size, clay mineral and elemental (Ti, Fe, Ca) compositions were measured for a core retrieved from a submarine fan in the Okinawa Trough. Varimax-rotated Principal Component Analysis (V-PCA) on time-evolution of grain size spectrum reveals that, since the Holocene, sediment was transported mainly by the benthic nepheloid layer (33%) and upper layers (33%) which is driven by the East Asian winter monsoon (EAWM). The intensification of the Kuroshio Current during the Holocene, masks the fluvial signal of the summer monsoon and obstructs clay minerals derived from the Yellow River, a major contributor prior to 12 ka BP. A new grain size index (GSI), which represents the EAWM well, exhibits a negative correlation with the $\delta^{18}O$ record in Dongge Cave, China during the Holocene when sea level was relatively steady. This anticorrelation suggests the southward migration of the Intertropical Convergence Zone (ITCZ). The consistency among our records and rainfall records in Peru, Ti counts in the Cariaco Basin, monsoon records in Oman and the averaged summer insolation pattern at 30°N further support the ITCZ's impact on monsoon systems globally. Cross-Correlation Analyses for GSI and log(Ti/Ca) against $\delta^{18}O$ record in Dongge Cave reveal a decoupling between the East Asian winter and summer monsoon during 5500–2500 cal yr BP, with greater complexity in the last 2500 years. This can be attributed to exacerbated ENSO mode fluctuations and possibly anthropogenic interference superimposed on insolation and ITCZ forcing.

1. Introduction

Monsoon systems play a pivotal role in the global distribution of heat and moisture. Monsoons affect more than one-third of world's population in numerous and varied ways, from agricultural irrigation to catastrophic disasters on an enormous spatial scale, such as flood or draught [*Maher and Hu*, 2006]. Remote sensing and direct observations indicate that monsoons are the manifestation of the seasonal migration of the Intertropical Convergence Zone (ITCZ) [*Gadgil*, 2003]. Long-term changes in monsoon intensity, such as the East Asian monsoon, are intimately related with the latitudinal migration of the ITCZ. The migration of the ITCZ is governed by precession forcing, i.e., a variation in insolation, an external forcing to climatic systems [*Shi et al*., 2012; *Wang*, 2009].

The East Asian monsoon is characterized by a moist southwesterly summer monsoon and a strong northwesterly or northeasterly winter monsoon [*Steinke et al*., 2011]. The East Asian winter monsoon (EAWM) basically involves the atmospheric flow above Asia which is related to the cold air originating from a high-pressure cell over Siberia and Mongolia [*Sone et al*., 2013]. On the other hand, ITCZ northward migration may enhance the East Asia summer monsoon (EASM). The inverse relationship between EAWM and EASM is discernable over the glacial-interglacial scale for the past 140,000 years [*Xiao et al*., 1995]. However, there is currently a serious debate raging over the existence of this inverse relationship during the Holocene. Recent studies of EAWM Holocene history based on aeolian dust flux in loess-paleosol [*An*, 2000; *Xiao et al*., 1995], various proxies in lacustrine [*Liu et al*., 2009; *Xiao et al*., 1997], marine sediments [*Tian et al*., 2010; *Xiao et al*., 2006] and stalagmite [*Sone et al*., 2013] can offer no consensus in explaining the variation of the EAWM, while not providing satisfactory evidence or a working hypothesis to link EAWM to EASM. *Yancheva et al*. [2007] found that the EAWM weakened during the early Holocene and intensified in the late Holocene, as a

response to the migration of the ITCZ which contemporaneously modulates the EASM. Such antiphase correlation was also further corroborated by a study in Tibet [*Liu et al*., 2009].

On the contrary, some studies based on temperature gradient, modeling efforts and diatom species abundance suggested in-phase or partially in-phase variation of the EAWM and EASM during the Holocene [*Steinke et al*., 2011; *Wang et al*., 2012; *Zhou and Zhao*, 2009]. These authors attributed the in-phase correlation to changes in seasonal insolation intensity since approximately 9000 cal yr BP [*Berger and Loutre*, 1991; *Wanner et al*., 2008], which leads to subsequent changes in sea-land contrast [*Dyke and Prest*, 1987; *Kutzbach et al*., 1998].

The most recent δ^{18}O research on stalagmites from Itoigawa, Japan revealed another instance of inverse correlation again for period of 10,000–5500 cal yr BP [*Sone et al*., 2013]. Further, a more complex correlation between the EAWM and the EASM in the last 5500 cal yr BP is evident, during which there is an instance (5200–4400 cal yr BP) of covariation which is attributed to the transformation from a migration of the ITCZ to a reduced seasonal insolation contrast as the dominate factor affecting the system [*Sone et al*., 2013]. The ambiguity of the relationships in the Holocene was also attributed to the low age resolution of the sampled core and the proxies used [*Steinke et al*., 2011; *Tian et al*., 2010].

The ENSO cycle which acts as an internal forcing, has been closely associated with Earth's climate since, at least, 130,000 cal yr BP [*Tudhope et al*., 2001]. However, the frequency of ENSO mode fluctuations during the last 5000 years is significantly higher than in the early to middle Holocene [*Conroy et al*., 2008; *Rodbell et al*., 1999]. The effect of ENSO has been identified as a source accountable for an out-of-phase EASM at the interannual and precession scales [*Shi et al*., 2012]. On the other hand, ENSO, since $\sim$5000 cal yr BP, has been responsible for the increased variability in summer monsoons recorded in δ^{18}O in Dongge Cave and in the fluvial runoff proxy documented by Ti counts in the Cariaco Basin [*Dykoski et al*., 2005; *Haug et al*., 2001]. Beside paleoclimate reconstructions using fossil corals, modeling has also revealed that there has been an increase in ENSO activity since 5000 cal yr BP and that ENSO variability has increased since 3000 cal yr BP [*Clement et al*., 2000; *Donders et al*., 2008; *Liu et al*., 2000; *Rodbell et al*., 1999]. Nevertheless, the imprint of ENSO since 5000 cal yr BP has not yet been adequately separated from the effects of ITCZ/insolation forcing and incorporated into any discussions on the dynamic relations between the EAWM and the EASM.

With the intention of shedding light on the aforementioned questions, we collected a sediment core from a deep-sea fan in the middle of the Okinawa Trough, a depocenter of winnowed sediments derived from the East China Sea which is located on the north edge of the ITCZ (Figure 1). The geographic and geomorphological features of the core site may hopefully help us reconcile the inconsistencies among the proxies and site-specific records which respond to the local or regional climate.

The purpose of this paper is to examine the evolution through time of sediment mineralogy and, thus, to infer the variation of ocean circulation patterns from the changes in mineralogy. Based on grain size data sets and in-depth statistical analyses, a new index is proposed to reflect the intensity of the winter monsoon. According to the index, we identify three transport mechanisms for particles of a specific grain size. A comparison of our records with others located near to the ITCZ is made to further assist in verifying our hypothesis of the ITCZ's modulation on the East Asian monsoon system, in which the effect of insolation and ENSO forcing is detailed.

2. Regional Setting

The Okinawa Trough is a curved basin behind the Ryukyu Arc in the northwestern Pacific (Figure 1). As a passage linking China to the west Pacific Ocean, the Okinawa Trough may serve as a rich and sensitive reflection of the environmental transition between the ocean and continental settings. During the last glacial period, when global sea level was relatively low and the climate was cooler and drier [*Clark et al*., 2009; *Lambeck and Chappell*, 2001; *Liu et al*., 2004], a large area of the East China Sea continental shelf was exposed and the coastline was progradational [*Saito et al*., 1998]. However, at that time, the Okinawa Trough remained submerged and sediments deposited there recorded the changing environment of the East China Sea [*Li et al*., 2001].

The climate of our study area is currently influenced by the East Asian monsoon system, which impacts the regional temperature, humidity, and atmospheric circulation [*Lee and Chao*, 2003]. In summer, the low air

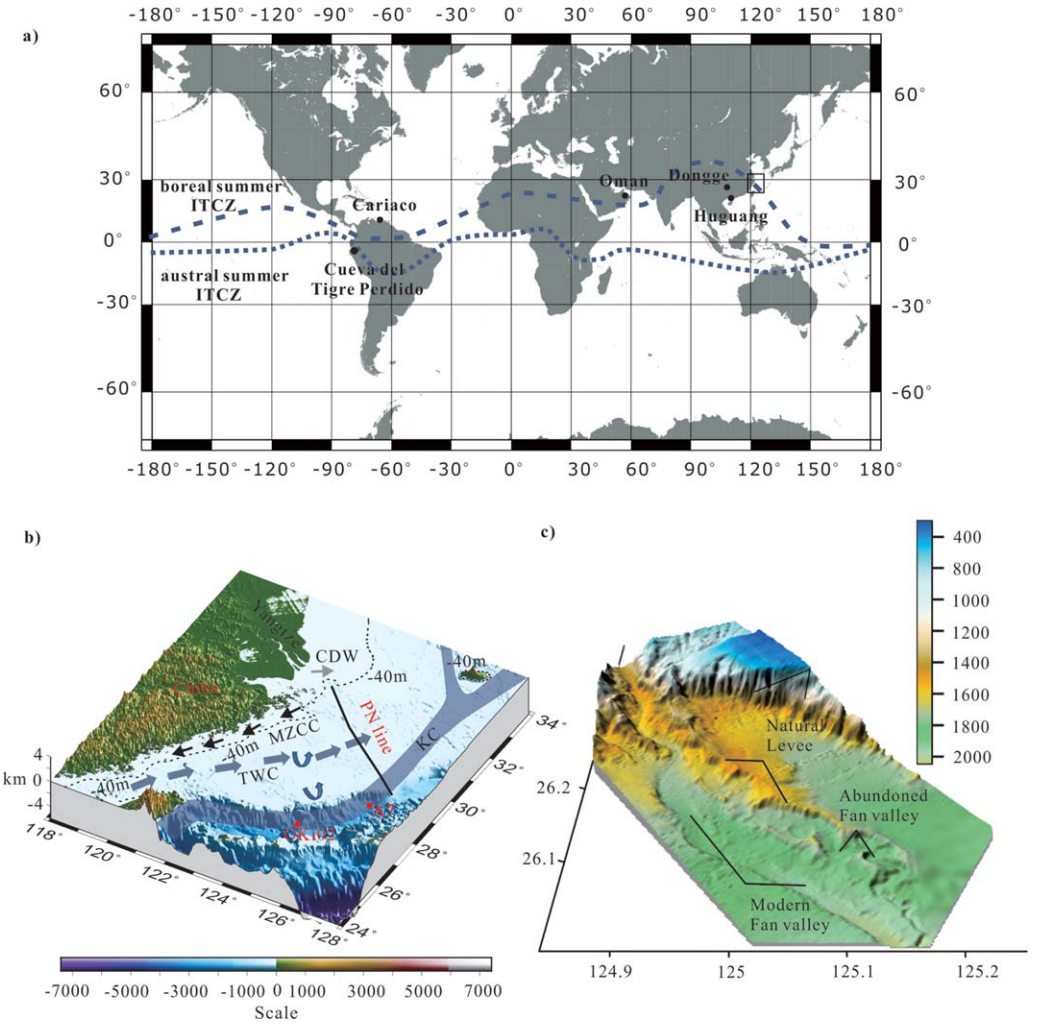

Figure 1. Schematic maps of (a) research area and data. The blue dash lines represent the boreal summer ITCZ and austral summer ITCZ, respectively; the black rectangle denotes the research area. (b) Regional circulation and bottom topography. CDW: Changjiang Diluted Water; MZCC: Minzhe Coastal Current; TWC: Taiwan Warm Current; KC: Kuroshio Current; PN line: major observational transect of project "MASFLEX." Red circles represent locations of Core Oki02 and A7. The black dash line shows the isobath of −40 m. The topographic map was created by GMT using ETOPO1 with 1 min precision. (c) Chiwei island canyon systems revealed by Multibeam bathymetric data [*Zhao et al.*, 2011], where the Core Oki02 was retrieved.

pressure above the central Eurasian continent causes southwesterly winds of approximately 5 m/s which carry warm and moist air from the Pacific Ocean toward Taiwan and Mainland China (Figure 2b). In winter, reversed pressure gradients favor northeasterly winds of approximately 12 m/s which bring cool and dry air from the Eurasian continent toward the Pacific Ocean, meanwhile, the ITCZ moves further south (Figures 1 and 2a). The seasonal variation of the monsoon system results in a significant change in the hydrographic conditions of the East China Sea and in the magnitude versus the main direction of Kuroshio Current east off of Taiwan. These factors combine to alter the volume of ocean water transported into the Okinawa Trough [*Diekmann et al.*, 2008; *Lee and Chao*, 2003; *Yuan and Hsueh*, 2010; *Yuan et al.*, 2008].

It has previously been demonstrated that the offshore sediment transport, in the present day, primarily occurs during the winter, when sediment bearing currents are driven by a prevailing northeasterly wind [*Iseki et al.*, 2003; *Yanagi et al.*, 1996]. The Ekman effect triggers downwelling, which when coupled with wind-driven mixing and tidally induced resuspension, induces a seaward near-bottom transport; whereas transport is inhibited by the transverse circulation pattern attributable to the Kuroshio Current's intrusion during the summer months [*Yanagi et al.*, 1996; *Yang et al.*, 1992]. In the present day, due to a summertime southward migration of the bifurcation position of the North Equatorial Current, the volume of ocean water

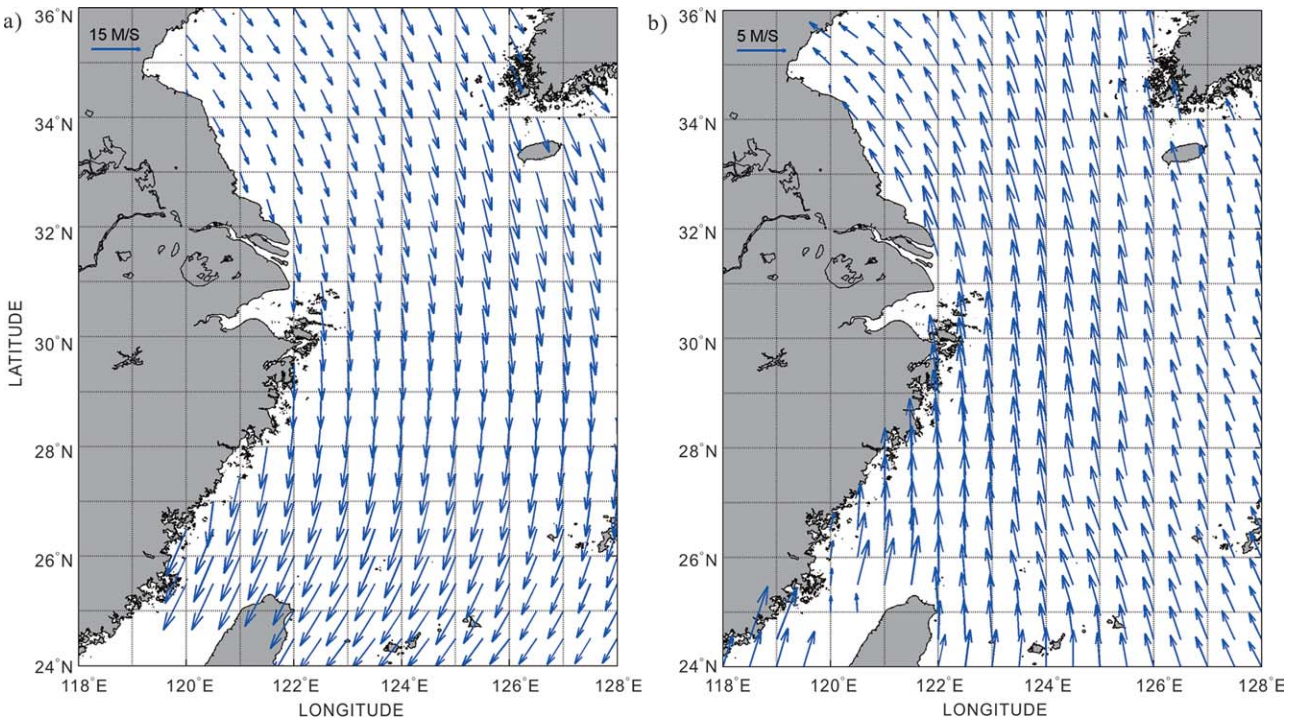

Figure 2. The monthly averaged wind speed field in East China Sea for (a) January 2011 and (b) July 2011 (http://www.ncdc.noaa.gov/thredds/OceanWinds.html?dataset=oceanwindsmon).

transported by the Kuroshio Current increases and is similarly reduced by the bifurcation position's winterly migration northward [*Kagimoto and Yamagata*, 1997; *Qu et al*., 2004; *Qu and Lukas*, 2003]. Thus, there is expected to be a teleconnection between the North Equatorial Current and the Kuroshio Current's downstream dynamics, which ultimately affects offshore sediment transport.

Furthermore, recent climate models and observations suggest that the EAWM is linked to ENSO [*Wang et al*., 2000]. Weak EAWM events occur during *El Niño* years and strong EAWM events occur during *La Niña* years [*Wang et al*., 2000]. The alternating ENSO modes could affect the winter circulation, which might also influence sediment delivery from the East China Sea to deep sea fans in the Okinawa Trough.

A series of submarine canyons distributed around the middle of the Okinawa Trough were revealed by multibeam bathymetric data and high resolution seismic survey by *Zhao et al.,* [2011] (Figures 1b and 1c). The site of Core Oki02 is located at the submarine fan linked to the Chiwei Island submarine canyon system which extends to the continental shelf break where depths are around −160 m (Figures 1b and 1c). The Chiwei Island canyon might serve as a conveyer belt for terrestrial/marine and lithogenic/biogenic materials to the Okinawa Trough [*Zhao et al*., 2011]. According to *Bouma* [2001], fine-grained submarine fans in the deep sea provide reliable paleoclimatological data by recording the variations in sediment transport and deposition. These variations are registered in the form of hypopycnal or hyperpycnal outflows triggered by climate change. Accordingly, the geographic and morphological features of Core Oki02 location might assist in the resolution of the dynamic relations between ENSO, the East Asian monsoon, and insolation input.

3. Materials and Methods

3.1. Materials

Core Oki02 (4.9 m, 125.20070 °E, 26.07359 °N) was retrieved from a water depth of 1612 m during "the autumn open offshore Cruise" by RV Science No I, belonging to the Institute of Oceanology, Chinese Academy of Sciences in September 2012 (Figures 1a–1c). Core Oki02 shows uniform lithology, containing primarily blue-gray clay silt with muddy lenses.

Table 1. Clay Mineral Assemblages for Core Oki02 and Potential Provenances

Sediments	Number	Smectite (%)	Illite (%)	Kaolinite (%)	Chlorite (%)	Kaolinite/Chlorite	Smectite/Illite
Oki02 (19.2–12 cal kyr BP)	118	8	67	10	15	0.64	0.13
Oki02 (12–0 cal kyr BP)	128	7	69	8	16	0.51	0.10
Yellow River	22	10	67	8	14	0.59	0.15
Yangtze	12	5	72	9	15	0.61	0.06
ECS	12	5	73	9	13	0.67	0.07
East of Taiwan[a]	4	0	75	3	23	0.13	0

[a]The samples of East Taiwan Rivers refers from *Li et al.* [2012].

3.2. Clay Mineral Analyses

Clay mineral (< 2 μm) analysis was performed at 2 cm intervals. To trace the source of clay minerals, we collected 22 samples from the Yellow River, 12 samples from the Yangtze River, and 12 samples from the East China Sea shelf (see Table 1; Figures 3 and 4). Pretreatment and measurements were based on the methods described by *Wan et al.* [2007]. After the removal of carbonate and organic matter, the clay minerals (<2 μm) were separated using the principle of Stokes' settling velocity. The extracted clay minerals (<2 μm) were smeared on glass slides after being fully dispersed by an ultrasonic cleaner, and they were then dried at room temperature. Semiquantitative estimates of the peak areas of the basal reflection for the main clay mineral group (smectite, 17 Å, illite, 10 Å, and kaolinite/chlorite, 7 Å) were carried out on the glycolated samples using Jade 5.0 software. The clay mineral abundances were estimated using the empirical factors of *Biscaye* [1965]. This method has been proven effective in provenance analysis conducted in recent years [*Wan et al.*, 2007; *Wan et al.*, 2010; *Wan et al.*, 2012; *Xu et al.*, 2009; *Xu et al.*, 2012]. The analysis error of replicate testing is around 6%.

3.3. Grain-Size Distribution of the Detrital Particles

The grain size analysis was conducted at 2 cm interval. The detrital fraction of the sediments was isolated from the bulk sediment after removal of the organic matter by hydrogen peroxide (15%), the carbonates by hydrochloric acid (0.5 mol/L), and the siliceous (opal, sponge spicule) by sodium hydroxide following the method of *Sun et al.* [2003]. Approximately 1 mL (0.05 mol/L) sodium metaphosphate was used to disperse the residual sample contained in a test tube while submerged in an ultrasonic cleaner for 1 min, and then analyzed with a Cilas 940L laser grain size analyzer at the Institute of Oceanology, Chinese Academy of Sciences. The detection limit was between 0.5 and 2000 μm. The analysis error of replicate testing is less than 3%.

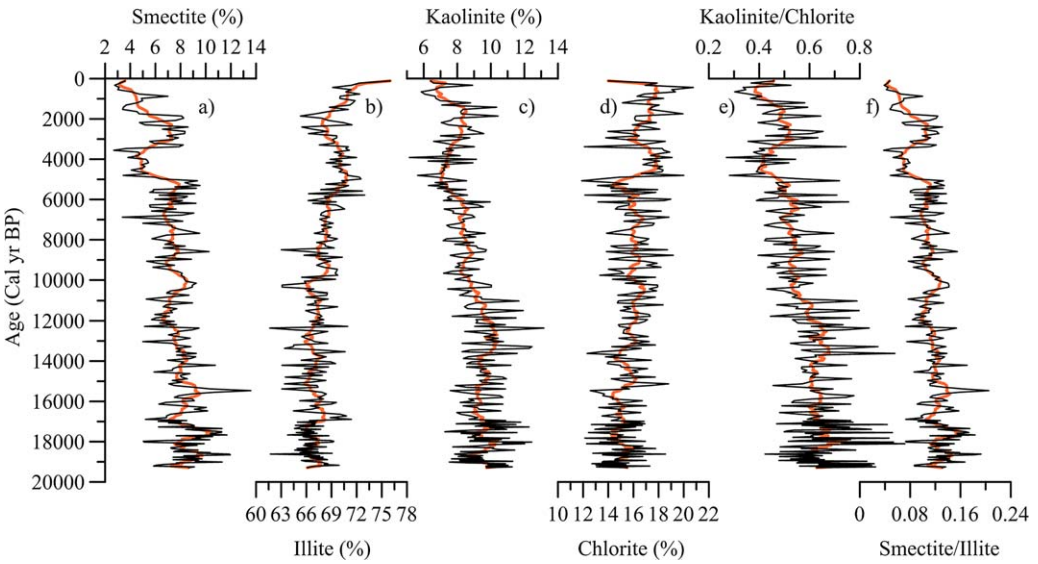

Figure 3. Secular variation of clay mineral assemblages (black curves, in %) and 5 points running averages (orange line) for (a) smectite, (b) illite, (c) kaolinite, (d) chlorite, (e) kaolinite/chlorite, and (f) smectite/illite of Core Oki02.

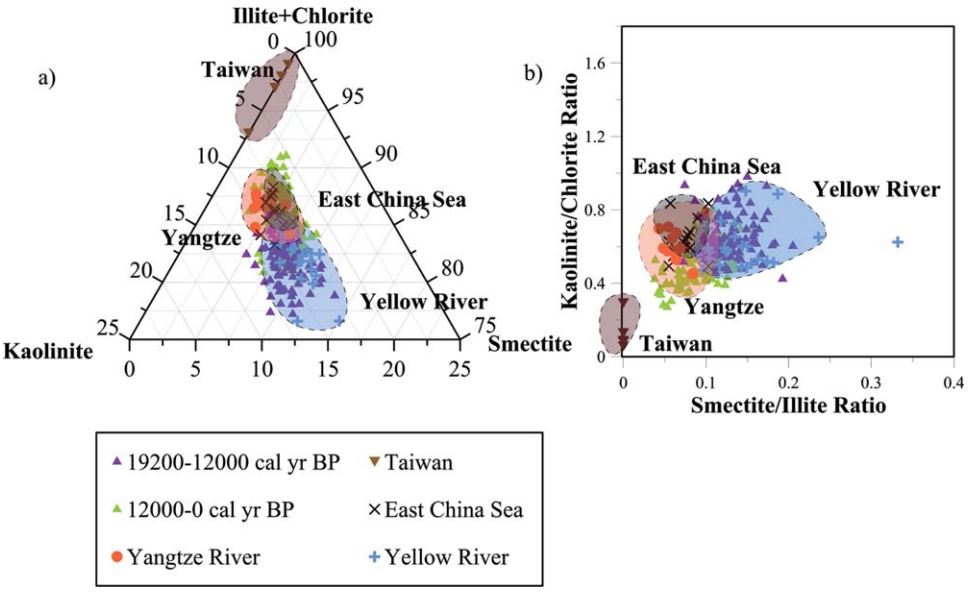

Figure 4. End member analysis of provenance using (a) a ternary diagram of smectite-kaolinite-(illite+chlorite) and (b) smectite/illite versus kaolinite/chlorite ratios. The green triangle represents an interval of 12,000–0 cal yr BP for Core Oki02; the violet triangle shows 19,200–12,000 cal yr BP; and the brown inverted triangle represents Taiwan River samples. The black crosses denote East China Sea Continental shelf samples, the orange circles are Yangtze River samples, and the blue crosses are Yellow River samples (also see Table 1).

3.4. Core Scanning

The major elemental compositions were measured with an Itrax X-ray fluorescence (XRF) core scanner. Measurements were carried out at 30 kV and 40 mA at 1 cm intervals. The elemental composition acquired by the XRF core scanner is given as count rates, which are based on the elemental intensity. Here we select Fe, Ti and Ca for discussion.

3.5. Age Model

The age model for Core Oki02 was constructed by 10 AMS ^{14}C dates. The AMS ^{14}C age was measured at the AMS laboratory, Beta Analytic. Mixed planktonic foraminifera shells were selected from fine-grained layers (see Table 2). The calendar ages were acquired by using Calib 6.0 with a reservoir age of 400 years [*Sun et al*., 2005; *Yoneda et al*., 2007]. The date for surface sample (0–2 cm) is 100.6 pMC, which is not consistent with the reservoir age. We suspect the foraminifera shells in surface sediments might contain bomb ^{14}C signal, yet, this would not influence our dates down core. The bottom layer of the sediment extends to approximately 19,200 cal yr BP (Figure 5).The sedimentation rates varied between 18 and 50 cm/cal kyr^{-1} (Figure 5). The high sedimentation rates and 1 cm sampling interval yield a temporal resolution of 20–50 years per sample, which is beneficial to climate change study at the centennial scale.

Table 2. AMS ^{14}C Ages Measured in Core Oki02[a]

Depth (cm)	Beta Lab Code	Conventional AMS 14C Age (yr BP)	Calendar Years (cal yr BP)	Date Resources
0–2	Beta-373510	100.6±0.3 pMC		Planktonic foraminifer mixture
52–54	Beta-337538	3150±30	(2891)2772–3012	Planktonic foraminifer mixture
104–106	Beta-373511	4920±30	(5203)5048–5299	Planktonic foraminifer mixture
134–136	Beta-373512	5830±30	(6222)6120–6294	Planktonic foraminifer mixture
162–164	Beta-337539	7200±40	(7631)7547–7741	Planktonic foraminifer mixture
188–190	Beta-373513	8300±30	(8815)8649–8961	Planktonic foraminifer mixture
212–214	Beta-373514	9230±40	(10,011)9833–10,162	Planktonic foraminifer mixture
248–250	Beta-337540	10560±40	(11,731)11,404–11,933	Planktonic foraminifer mixture
372–374	Beta-337541	14290±50	(16,932)16,763–17,130	Planktonic foraminifer mixture
488–450	Beta-337542	16530±60	(19,230)18,938–19,429	Planktonic foraminifer mixture

[a]pMC: percent modern carbon.

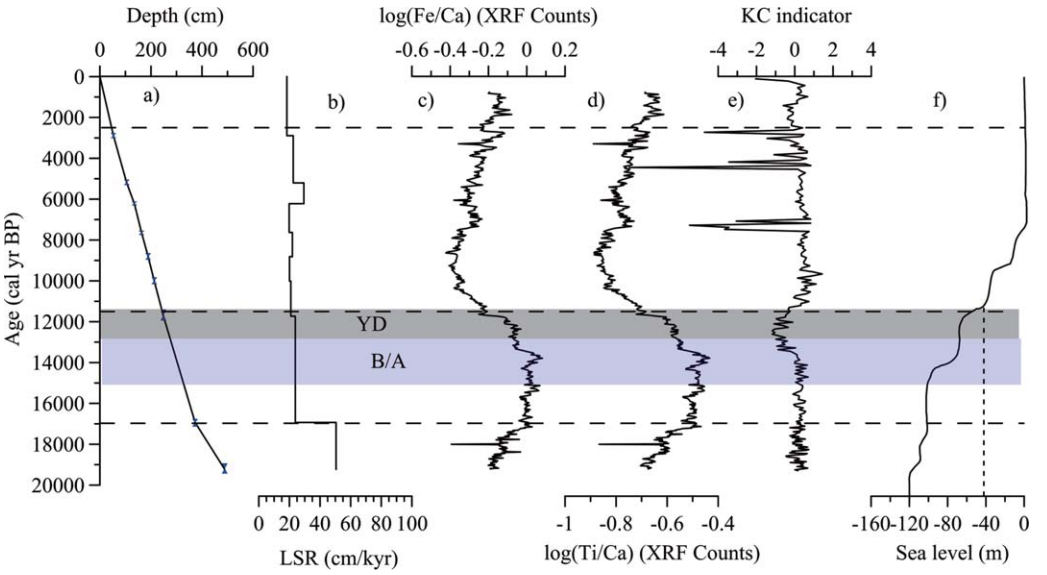

Figure 5. (a) Calendar ages against depth for Core Oki02, the uncertainties are plotted at the 2δ level (blue bar); (b) linear sedimentation rate; (c) log(Fe/Ca); (d) log(Ti/Ca), (e) Kuroshio Current indicators extracted from grain size analysis of Core Oki02; (f) Sea level variation in the western Pacific since LGM [*Liu et al*., 2004].

3.6. Statistical Analyses

3.6.1. Varimax-Rotated Principal Component Analysis

Varimax-rotated Principal Component Analysis (V-PCA) was applied to time variation of grain size spectrum with the input grain size matrix ranging from 0.5 to 71 μm (Figure 6). PCA is a statistical procedure that uses orthogonal transformation to convert a set of possibly correlated variables (grain size sets) into a set of linearly uncorrelated variables (grain size sets) called principal components. This method allowed us to separate out orthogonal modes, independent grain-size spectra, from the grain size matrix that are related to potential input functions and sensitive to specific transport mechanisms [*Darby et al*., 2009]. V-PCA has been used to successfully differentiate sea ice, bottom current transports in the Arctic Ocean, and also acquire a fluvial proxy to reconstruct East Asian monsoon history in the Bohai Sea, China [*Darby et al*., 2009; *Yi et al*., 2012]. The mode of each extracted grain size component is defined as the grain size sets with largest factor loading, which is most representative for the grain size spectra (Figure 6). According to *Darby et al*. [2009], specific mechanisms may result in the unique grain size spectra, which are provided by the specific grain size associated with sea ice-rafted and bottom current.

To verify the applicability of this method in the Okinawa Trough, we have conducted V-PCA on the grain size data of the sediments of cores Oki02, A7 in the Okinawa Trough, inner and outer East China Sea continental shelf (X.F. Zheng, unpublished data). Our validations confirm that cores Oki02 and A7 in the Okinawa Trough share the same data structure which is seen by nearly identical factor loading models, but differ from that of inner and outer continental shelf sediments (X.F. Zheng, unpublished data). The distinctive features between the extracted grain size spectra from the cores in the Okinawa Trough and from the sediments in the East China Sea continental shelf is attributable to the transport mechanisms that control the patterns of grain size spectrum. This validation gave us confidence that the V-PCA could identify transport mechanisms.

3.6.2. Cross-Correlation Analysis

Cross-Correlation Analysis (CCA) is a powerful tool in assessing the long range cross correlation between two nonstationary data sets. CCA has been successfully used in hydrological and delta hydrogeomorphology studies [*Hajian and Movahed*, 2010; *Marriner et al*., 2012]. To establish whether the relationship of teleconnection mentioned above exists among records, CCA ($P<0.05$) was applied to our newly proposed index (GSI, see below), log(Ti/Ca) and the $\delta^{18}O$ of stalagmite in Dongge Cave at three intervals (12,000–5500, 5500–2500, 2500–0 cal yr BP) using the free software "R." Equal time intervals (50 year) are adopted in our analysis in order to quantify the power-law cross correlations in the nonstationary time series [*Marriner et al*., 2012]. Correlation coefficients based on the lag 0 value within significant levels are considered.

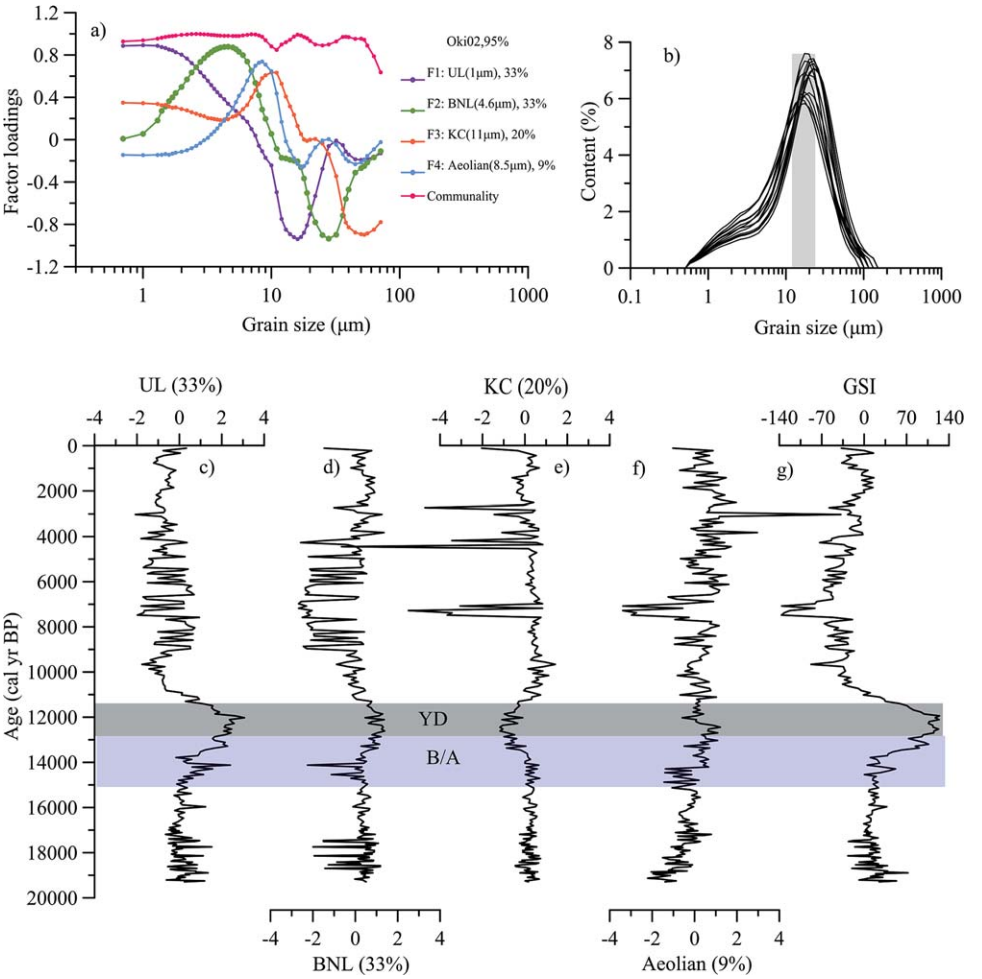

Figure 6. (a) F1, F2, F3, and F4 represent the components of V-PCA procedures and their variances. Note F1 (UL: upper layers transport), F2 (BNL: benthic nepheloid layer), F3 (KC: Kuroshio Current), F4 (Aeolian deposit); (b) Grain size distribution of samples collected from Taiwan river during flood of Typhoon Mindulle 2004; Secular variation of (c) F1, (d) F2, (e) F3, and (f) F4, (g) grain size Index (GSI).

3.6.3. Wavelet Analysis

Wavelet analysis was applied to the GSI, log(Ti/Ca) and Dongge stalagmite δ^{18}O time series. Wavelet analysis allows an automatic localization of cyclic patterns, both in time and frequency [*Torrence and Compo*, 1998]. In this analysis, we chose the Morlet wavelet with a wave number of six to identify large scale changes in variance within selected frequency bands through time. Before the Morlet wavelet power spectrum analysis, the GSI, log(Ti/Ca) and δ^{18}O of stalagmite in Dongge was resampled at a 20 year resolution, and filtered to remove false cycles.

4. Results and Discussion

4.1. Clay Minerals and Implications for Provenance

The proportional distribution profiles of four major clay minerals from Core Oki02 are shown in Figures 3 and 4. The clay mineral assemblages are composed of illite (65–74%), chlorite (13–19%), smectite (3–11%) and kaolinite (6–11%). According to the variations of the clay mineralogy, the core can be divided into three parts. During 19,200 to 12,000 cal yr BP, the illite, kaolinite, smectite and chlorite contents were stable and varied with a small amplitude. From 12,000 to 5500 cal yr BP, kaolinite decreased gradually, while illite and chlorite increased correspondingly. For the recent time periods, 5500 cal yr BP, clay mineral assemblages are more variable. Note that the proportion of kaolinite and smectite diminished in conjunction, while illite and chlorite increased since 2500 cal yr BP (Figures 3 and 4).

Based on clay mineralogy and biogeochemical/geochemical proxies previous studies indicated that terrigenous clastic sediments deposited in the middle of the Okinawa Trough mainly originated from 1) Yangtze River, 2) Yellow River, 3) mountainous rivers in the east Taiwan and 4) the East China Sea continental shelf particularly during low sea level stand [*Hoshika et al*., 2003; *Diekmann et al*., 2008; *Dou et al*., 2010; *Dou et al*., 2012; *Iseki et al*., 2003; *Kao et al*., 2008a, 2008b] and, also, that the fractional contributions from the 4 sources varied through the glacial-interglacial cycle. The clay mineral assemblages in the Yangtze River predominantly consist of illite (67–75%, averaging 72%) and chlorite (11–18%, averaging 15%), with lesser amounts of kaolinite (7–11%, averaging 9%) and smectite (3–8%, averaging 5%) (see Table 1 and Figure 4). The Yellow River known for having the highest sediment load on earth (approximately 1×10^9 t/yr), has also contributed tremendously to the study area since the late Quaternary [*Milliman and Meade*, 1983; *Milliman and Syvitski*, 1992]. The Yellow River mainly contains illite (58–71%, averaging 67%) and smectite (7–19%, averaging 10%), with lesser quantities of chlorite (11–17%, averaging 14%) and kaolinite (7–12%, averaging 8%) (see Table 1 and Figure 4). The clay mineral assemblages of the Yellow River sediments are comparable to those of the Yangtze River, although the Yellow River samples have a higher smectite content and higher mineral crystallinity [*Yang et al*., 2003]. As for the East China Sea continental shelf, the sediment is composed mainly of illite (68–78%, averaging 73%) and chlorite (10–16%, averaging 13%), with scarce smectite (4–7%, averaging 5%) and kaolinite (8–11%, averaging 9%) (see Table 1 and Figure 4). In Taiwan, strong tectonic activity, rapid uplift and frequent high energy storms result in one of the highest soil erosion rates in the world [*Li et al*., 2012; *Li*, 1976]. Previous studies indicate that sediments exported to the Okinawa Trough are derived mainly from rivers in eastern Taiwan where they collectively discharge up to 150 Mt/yr [*Diekmann et al*., 2008; *Liu et al*., 2008]. Sediments from Taiwan are transported northward by the Kuroshio Current situated on the east side of Taiwan [*Diekmann et al*., 2008; *Dou et al*., 2010]. The clay mineral assemblages for the eastern Taiwan rivers consist of illite (74%) and chlorite (22%) with an absence of smectite and kaolinite (4%) (see Table 1 and Figure 4) [*Li et al*., 2012].

Assuming that the clay mineral assemblages of the sediment provenances were essentially stable since the last glacial period, we may distinguish the clay mineral sources in different time periods by using smectite/illite versus kaolinite/chlorite ratios and a ternary diagram of three components: smectite, kaolinite and (illite+chlorite) (Figures 4a and 4b). We found that during 12,000–0 cal yr BP most samples fall in the field close to the East China Sea continental shelf and the Yangtze River provenance, but deviate from the compositions of the Taiwan and Yellow River sediments (Figures 4a and 4b). During 19,200–12,000 cal yr BP, the clay minerals were derived mainly from the Yellow River, the Yangtze River and the East China Sea continental shelf with less contribution from Taiwan (Figures 4a and 4b). Accordingly, we conclude that the clay minerals of Core Oki02 originated mainly from the rivers of the China's mainland with lesser amounts coming from Taiwan throughout the last 19,000 years. The absence of clay components from the Yellow River in the Holocene period may be attributed to the enhanced Kuroshio Current and the formation of modern current systems (e.g., water barrier). Interestingly, although a remarkable sea-level change had occurred during the period from 15,000 to 12,000 cal yr BP [*Liu et al*., 2004], we do not observe a significant change in the clay mineral assemblage for this specific time period. Thus, the effect of sea level may have played a secondary role in sediment transport to the middle Okinawa Trough (Figure 3). The relatively steady sea level during the Holocene minimizes its impact on East China Sea circulation patterns [*Kao et al*., 2006], thus, allowing monsoons to more effectively force the delivery of sediment to deep sea fans.

On the other hand, since kaolinite is absent in the rivers of Taiwan, but found at relatively higher proportions in the rivers of mainland China [*Li et al*., 2012], the variation of kaolinite itself, to some extent, could be used to monitor the relative terrigenous contribution from mainland China in spite of the dilution effects that could influence the abundance of kaolinite [*Wang et al*., 2013].

4.2. Features of the Grain Size Spectrum and Transportation Mechanisms

Four components (F1, F2, F3, and F4) were identified to explain $\sim$ 95% of the total amount of variance in Core Oki02 (Figure 6a).The first mode (F1) accounting for 33% of the variance has a positive broad peak at 1 μm and an anticorrelated negative peak at 15 μm (Figure 6a); the second mode (F2) for 33% has a positive peak at 4.6 μm and large anticorrelation at about 30 μm (Figure 6a). The third mode (F3) for 20% contains a peak at 11 μm and moderately strong negative loadings above 40 μm (Figure 6a). The fourth mode (F4) for 9% has a positive peak at 8.5 μm (Figure 6a). As mentioned earlier, the Core A7 gave the same modes with

a consistent grain size structure, such consistency strongly indicates that there must be identifiable mechanisms to account for the four specific modes.

Terrigenous particles that settled in the marine environment are regarded as mixed materials that are derived from various sources and experience different transport processes, which may lead to distinctive grain-size distributions [*Darby et al*., 2009]. According to previous research, five processes associated with various sediment sources dominate in the East China Sea. These are resuspended sediments carried by the benthic nepheloid layer (BNL), fine sediments transported in the upper layers (UL) of the water column on shelf [*Iseki et al*., 2003], sediments from Taiwan and/or East China Sea continental shelf carried by Kuroshio Current [*Diekmann et al*., 2008; *Hsu and Hanes*, 2004], turbidity currents triggered by submarine earthquakes [*Huh et al*., 2004], and volcanic eruptions [*Machida*, 1999].

F3 (11 μm) is interpreted as an indicator of the Kuroshio Current. This is due not only to grain size itself but also because of its contribution to the variance in several cores (Figure 6a). The down-core variation of the factor score of F3 agrees well with the patterns of sortable silt (10–63 μm) among Core Oki02, cores A7 and ODP1202 (X.F. Zheng, unpublished data) (Figure 6e). According to *McCave et al.* [1995], the mean size and percentage of sortable silt (10–63 μm) are good indicators of paleocurrent winnowing because its noncohesive property which allows it to be easily sorted or transported by currents [*McCave et al*., 1995]. The F3 mode of 11 μm is close to the mean size (14 μm) of sortable silt (10–63 μm) [*McCave et al*., 1995]. In addition, the secular variation of F3 in Core Oki02 is concordant with the percentage variation of *P.obliquiloculata* in Core A7, an indicator of the Kuroshio Current [*Xiang et al*., 2007] (Figure 6e). The transport mode of 11 μm can be evaluated by the Rouse number. The Rouse number ($R_0 = Ws/\kappa U^*$) is a nondimensional parameter in fluid dynamic which is used to determine how sediment will be transported in a flowing fluid. R_0 expresses the ratio of settling velocity to the shear velocity; Ws is the settling velocity of the grains, κ is the von Karman constant (0.4), and U^* is the boundary shear velocity. R_0 values $>$2.5 indicate bed load transport, a value between 2.5 and 1.2 indicates that 50% of sediment is transported in suspension, while the range 1.2 to 0.8 indicates 100% suspension, and a Rouse number less than 0.8 denotes a fully suspended wash load. The Rouse number indicates that the 11μm will be transported in the Kuroshio Current by suspension (X.F. Zheng, unpublished data). The sediment discharge during the floods of the largest Taiwan river is composed mainly of mud with a mean size of $\sim$10 μm [*Kao et al*., 2008a] (Figure 6b), which might act as a supplier for the 11 μm sediment carried by the Kuroshio Current. Thus all of these factors suggest that F3 indicates the sediment transported by the Kuroshio Current.

The other two main mechanisms for sediment transport to the Okinawa Trough are the benthic nepheloid layer and upper layers, which are controlled by winter monsoons [*Hoshika et al*., 2003; *Bian et al*., 2010; *Iseki et al*., 2003; *Oguri et al*., 2003]. Transport by BNL is a key process to export shelf material to deep sea [*Iseki et al*., 2003] and BNL are typically driven by northeasterly prevailing winds [*Bian et al*., 2010; *Yanagi et al*., 1996; *Yang et al*., 1992]. Sediments discharged from the Yangtze River during summer floods are confined mainly to the subaqueous delta and inner shelf. A smaller portion is transported northeastward carried by the Taiwan Warm Current mingled with intruding Kuroshio subsurface water, which becomes a "water barrier" for offshore transport [*Bian et al*., 2010; *Yang et al*., 1992]. The "water barrier" is weakened in the winter or even terminated by intensified northeasterly winds [*Yang et al*., 1992; *Yuan et al*., 2008]. The downwelling forcing, coupled with vigorous mixing driven by winter monsoon facilitate both BNL and UL transportation to the Okinawa Trough [*Bian et al*., 2010; *Iseki et al*., 2003; *Oguri et al*., 2003; *Yanagi et al*., 1996].

Here we infer that F1 (1 μm) and F2 (4.6 μm) are indicators for UL and BNL, respectively (Figure 6a). According to clay mineral analysis, the clay minerals ($<$2 μm) of Core Oki02 are derived mainly from the Yangtze River, the Yellow River and the East China Sea continental shelf, with lesser amounts derived from Taiwan Island (Figures 3 and 4). On the other hand, the mode of F2 (4.6 μm) is close to the reported medium grain size ($\sim$6 μm) of BNL in East China Sea [*Hoshika et al*., 2003]. The secular variation of the factor score of F1 is in phase with that of F2, indicating that they are governed by the same forcing (Figures 6c and 6d).

Sediments in canyon systems follow two primary transport pathways, namely shallow plume (of approximately 600 m) and near-bottom transport [*Kineke et al*., 2000; *Liu et al*., 2013]. These were observed in a canyon study done in the southern Okinawa Trough [*Hsu et al*., 2006]. Our inference is also consistent with the observations of a sediment trap and surface sediments collected from the middle of the Okinawa Trough along the PN line (Figure 1) [*Iseki et al*., 2003; *Oguri et al*., 2000].

It is very probable that the F4 (8.5 μm) of Core Oki02 represents the aeolian dust derived from Asian continental (Figure 6a). The mode and grain size spectra of F4 is close to that of aeolian dust (8μm), as revealed from a grain size analysis study of core MD01-2407 in the Japan sea and the aeolian dust sampled at Sapporo, Hokkaido in March 2002 [*Nagashima et al*., 2007]. In addition, the average terrigenous mass accumulation rates of Core Oki02 since 19,200 cal yr BP is 220 g m^{-2} annually. According to *Hsu et al*. [2009], the estimated dust deposition to East China Sea is 20 g m^{-2} annually. Thus, the maximum aeolian contribution may account for only 9% of the terrigenous flux in Core Oki02, which resembles the 8.9% variance contribution of F4. Interestingly, the secular variation of F4 is in phase with F1 and F2 before the Holocene (Figure 6), however, the covariance became insignificant in the Holocene. This Holocene disconnection is likely due to the enhanced northward Kuroshio Current and the Taiwan warm current, which might influence the settling of aeolian dust to the sea floor and thus diminish the variation of F4 (Figure 6).

4.3. Environmental Controls on Transport and Sedimentation

The down-core distribution of the iron/calcium (Fe/Ca) and titanium/calcium (Ti/Ca) ratios in the Core Oki02 are displayed in Figure 5. Elemental ratios are more useful than single elements due to their insensitivity to closure effects [*Weltje and Tjallingii*, 2008]. The ratios of Fe/Ca and Ti/Ca are commonly used to indicate influx of terrigenous material in marine sediments and thus, to reconstruct paleoclimate [*Arz et al*., 1998; *Arz et al*., 1999]. To reduce the influence of sample geometry and physical properties such as effects of specimen inhomogeneity, variable water interactions, grain-size distribution, and a general lack of control on measurement geometry, we utilized log(Ti/Ca) and log(Fe/Ca) as proxies. This provided interpretable data of the relative changes in chemical composition and eliminated the constant-sum constraint [*Weltje and Tjallingii*, 2008]. On the other hand, log(Ti/Ca) is positive correlated to log(Fe/Ca) suggests that Fe and Ti, as terrestrial elements, have same origin. As we can see from Figure 5, the linear sedimentation rate of Core Oki02 has been relatively constant since 16,000 cal yr BP. The marine material influx to the middle of the Okinawa Trough has also been stable since the beginning of the Holocene, as revealed by stable biogenic components, including $CaCO_3$ and opal contents, and the total organic carbon accumulation rate in the nearby Core DGKS9604, also located in the Okinawa Trough [*Dou et al*., 2011]. The stable accumulation rate may imply a constant sum of terrigenous and marine materials and thus further support the credibility of the usage of log(Ti/Ca) and log(Fe/Ca) as indicators for the terrigenous influx (Figure 5).

Down-core variations of terrigenous influx as indicated by log(Ti/Ca) are shown in Figure 5. During 19,200–15,000 cal yr BP, the sea level was low and the paleochannel was situated closer to the Okinawa Trough, concurrently, the Kuroshio Current was relatively weak as is indicated by low F3, which provided favorable conditions for the export of fluvial sediments, and thus causes the higher log(Ti/Ca) and F2 (bottom nepheloid layer transport) [*Saito et al*., 1998; *Wellner and Bartek*, 2003; *Xu and Oda*, 1999] (Figures 5 and 6). In the same time period, lower F1 (upper layer transport) may be overwhelmed by sediments transported higher in the water as F2 (bottom nepheloid layer transport) due to the shorten distance from the estuary and the high turbid of fluvial sediment [*Saito et al*., 1998; *Wellner and Bartek*, 2003]. Between 15,000 and 12,000 cal yr BP, rapid coastline retreat and submerging continental shelf, coupled with an immature Kuroshio Current, had created a better condition for BNL and UL transports, as indicated by the increase of F1 and F2; during the same time strong sediment reworking and erosion at the shelf edge since 15,000 cal yr BP was observed in the South and East China Sea [*Dou et al*., 2010; *Steinke et al*., 2008]. In this period, the increased distance from the estuary might diminish the fluvial supply resulting in marginal decrease of log (Ti/Ca) [*Saito et al*., 1998; *Wellner and Bartek*, 2003].

During the Holocene, the Kuroshio Current initially gained strength and then rapidly attained stability which it maintained throughout the Holocene (X.F. Zheng, unpublished data) (Figure 7). According to numerical modeling research, the flow path and volume of the Kuroshio Current resembled present condition since the beginning of the Holocene, when the sea level was above −40 m [*Kao et al*., 2006; *Lee et al*., 2013] (Figure 1a). A shift in sediment provenance since the Holocene also suggests that the formation of a modern current system in East China Sea in response to an enhancement of the Kuroshio Current, which is linked to the Kuroshio Current branching out into the Japan Sea during the period from 11,500 to 8500 cal yr BP [*Xu and Oda*, 1999] (Figures 3 and 4). Based on planktonic foraminiferal records, during the period of 11,500–9000 cal yr BP, the coastal waters shift toward being dominated by the Kuroshio Current [*Xu and Oda*, 1999]. A drastic decrease in log(Ti/Ca) located in this transitional period supports the "Kuroshio Current water barrier" theory (Figure 7). According to grain size and clay mineral analysis, the sources of the clay

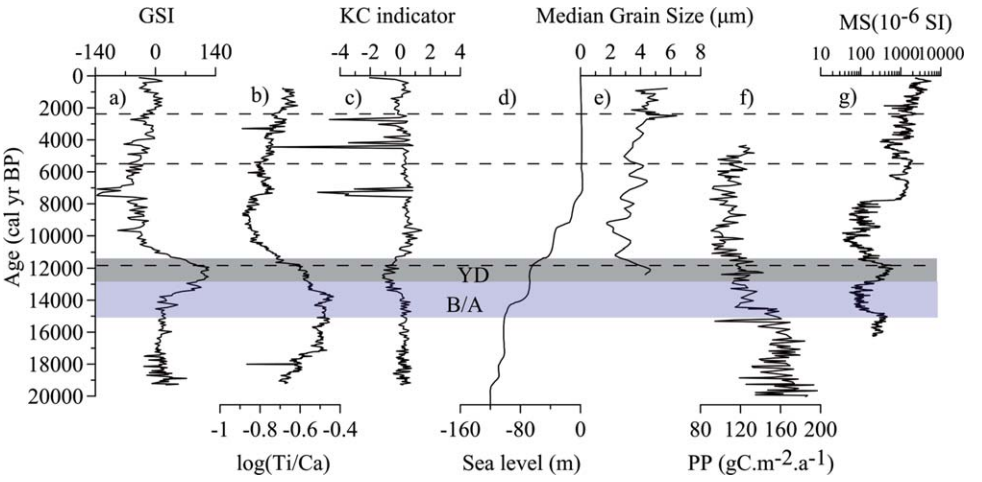

Figure 7. Temporal variations of (a) grain size Index (GSI), (b) log(Ti/Ca), and (c) Kuroshio Current (KC) indicator for Core Oki02. (d) Sea level pattern in the western Pacific since LGM [*Liu et al*., 2004], (e) Median grain size of loess in Duowa, western China [*Maher and Hu*, 2006], (f) Primary production in the Sulu sea [*de Garidel-Thoron et al*., 2001], (g) Magnetic susceptibility of sediment core in the Huguang Marr lake, Zhanjiang, China [*Yancheva et al*., 2007].

minerals were the Yangtze River and the East China Sea continental shelf, with a lesser contribution coming from Taiwan (Figures 3 and 4). Hence, the variation of log(Ti/ca) may reflect the relative contribution of terrigenous influx from mainland China in the winter since the Holocene (Figure 7).

In order to examine the EAWM pattern in the Holocene, we combined F1 and F2 into a new series of grain size index (GSI) based on their variance contributions (Figure 6f):

$$GSI = BNL \times 33 + UL \times 33 \quad (1)$$

The temporal pattern of the GSI during the Holocene agrees well with various EAWM proxies, including primary production in Sulu sea, median grain size of Duowa loess in western China and magnetic susceptibility in Huguang Marr lake, Guangdong, China [*de Garidel-Thoron et al*., 2001; *Maher and Hu*, 2006; *Yancheva et al*., 2007] (Figure 7). These agreements further support the credibility of interpreting GSI as an indicator of EAWM.

The GSI diminishes greatly since the Holocene and reaches a minimum at ~ 11,000–9000 cal yr BP, indicating that the BNL and UL transport were weakest (Figure 7). The GSI gradual decrease fully accords with the reported timing of northward shift and permanence of the ITCZ position in the winter [*Haug et al*., 2001; *Yancheva et al*., 2007] (Figure 7). The decreasing trend of log(Ti/Ca) since 12,000 cal yr BP further supports the gradually weakening of EAWN intensity in early Holocene (Figure 7). The decrease in percentage of kaolinite, which stands for the source material from mainland China, also supports an attenuation of the EAWM (Figure 3).

From 9000 to 5500 cal yr BP, a relatively low and steady GSI is concordant with a relatively low log(Ti/Ca), indicating a small terrigenous input, when the summer insolation in northern hemisphere was maximum [*Berger and Loutre*, 1991] (Figures 7, 8, and 9a). Mainland East China's contribution of kaolinite was initially steady and then begins to decrease (Figure 3). On the other hand, a high GSI is coeval with an ascending log(Ti/Ca) between 5500 and 2000 cal yr BP, which indicates a simultaneous increase in terrigenous influx via BNL and UL (Figure 7). The percentage of kaolinite also increased in this period (Figure 3). The concomitant variations in the GSI, log(Ti/Ca) and kaolinite nearly throughout the entire Holocene illustrate that the sediment dispersal was governed by the intensity of EAWM.

Since 2000 cal yr BP, the GSI has increased and scaled back in a short period, which is also evinced by synchronous variations in kaolinite (Figures 3 and 7). The log(Ti/Ca), however, shifted to a higher value and remained steady (Figure 7).

Based on the magnified variability in GSI and log(Ti/Ca) in the past 5500 cal yr BP, we inferred a larger century-scale variation of the EAWM (Figures 7 and 8), especially between 4500 and 2500 cal yr BP, which

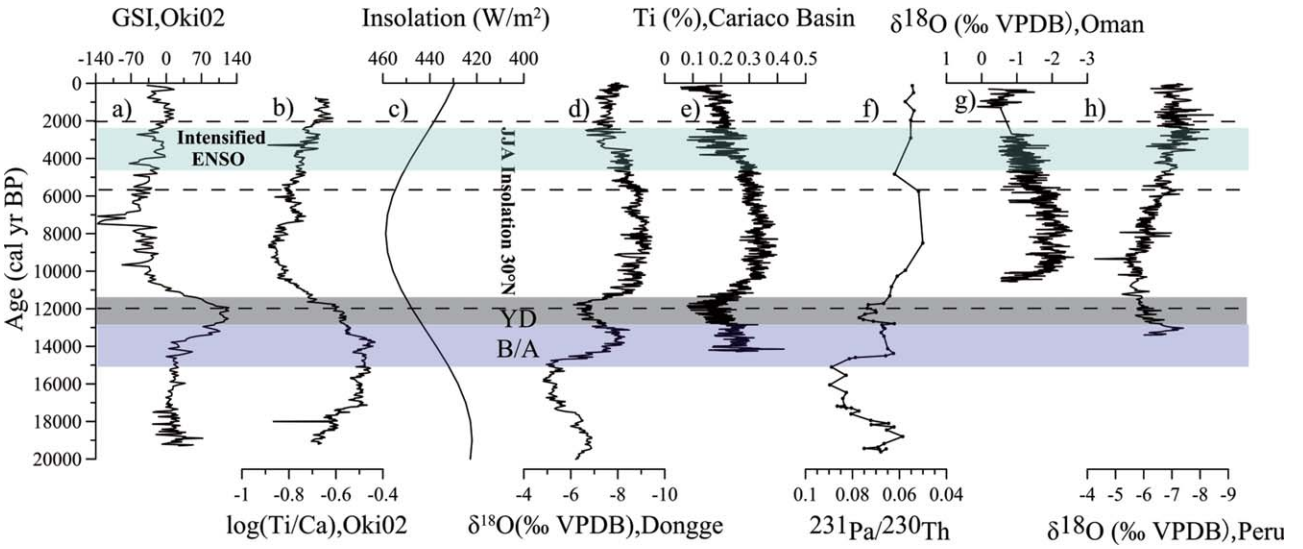

Figure 8. Records of (a) grain size Index (GSI), (b) log(Ti/Ca) of Core Oki02, (c) Insolation at 30°, averaged from June to August (JJA) [*Berger and Loutre*, 1991], (d) East Asian summer monsoon as indicated by δ^{18}O of stalagmite in Dongge Cave [*Dykoski et al*., 2005], (e) Fluvial runoff as indicated by Ti counts in Cariaco basin [*Haug et al*., 2001], (f) Atlantic Meridional overturning circulation as indicated by ^{231}Pa/^{230}Th in Bermuda rise [*McManus et al*., 2004], (g) Indian summer monsoon as indicated by δ^{18}O of stalagmite in Oman [*Fleitmann et al*., 2003], (h) Rainfall amounts as indicated by δ^{18}O of fossil drip water of stalagmite in Peru [*Van Breukelen et al*., 2008].

had been affected by the intensified ENSO activity (more *El Niño*) [*Haug et al*., 2001]. In fact, the southward migration of the ITCZ over the late Holocene was accompanied by the prevalence of *El Niño* because the northern hemisphere insolation became less seasonal while the southern hemisphere became seasonal [*Haug et al*., 2001].

A modeling study of contemporary conditions showed that the warm events (cold) in the eastern Pacific may result in weak (strong) EAWM due to the formation of an anticyclonic (cyclonic) system in the Pacific Ocean [*Wang et al*., 2000], which results in high frequency variation of the EAWM. Thus warm events (*El Niño*) may result in a weaker winter circulation in the East China Sea (Figure 9b), while cold events (*La Niña*) result in a strong winter circulation (Figure 9c). The rapid alteration of ENSO modes will apparently alter the sedimentation processes in the East China Sea. Below, we attempt to separate the signals modulated by the ITCZ and ENSO.

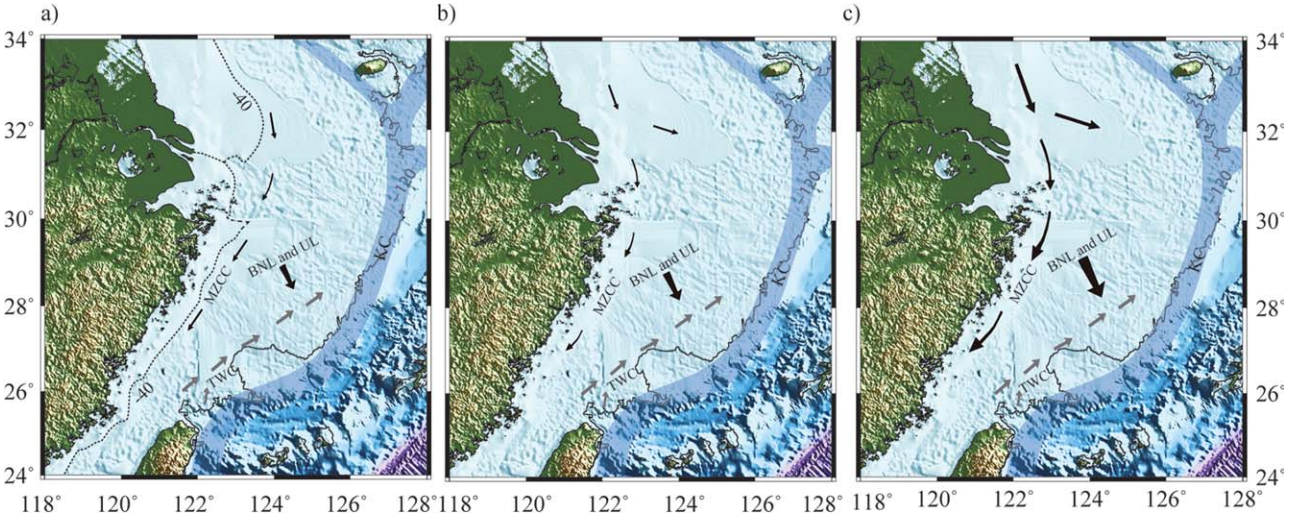

Figure 9. Scenarios of detrital sediment delivery conditions in the Okinawa Trough during (a) Insolation maximum, (b) *El Niño*, and (c) *La Niña* stages.

4.4. The Variation of East Asian Winter Monsoon: ITCZ Force and ENSO Modulation

The temporal variation of the GSI and log(Ti/Ca) of our marine sediment record, coupled with the Holocene EASM record in Dongge Cave, which have a similar latitude on land, supports the anticorrelation hypothesis by *Yancheva et al*. [2007] (Figure 8). As shown in Figure 8, the temporal patterns of the GSI and log(Ti/Ca) reveals an increasing trend from the early Holocene toward the late Holocene, while the pattern of the EASM record in Dongge shows a decreasing trend.

The disagreement between the competing hypotheses, that of the land-sea thermal contrast and the ITCZ, is likely dependent on which mechanism drives the East Asian monsoon system, namely, whether it is an internal or external forcing mechanism [*Wang*, 2009; *Yi et al*., 2012]. Internal forcing model suggest that the global ice volume exert a significant influence on the Asian monsoon by modulating the thermodynamic contrast between the Asian continent and the Pacific Ocean [*An et al*., 1990]. Conversely, the external forcing of solar insolation regulates the monsoon by substantially driving the ITCZ away from the equator (more than 10°); it is also suggested that the existence of ITCZ is not dependent on the land-sea contrast, rather the land-sea contrast determines a favorable longitudinal location for the ITCZ [*Chao and Chen*, 2001; *Yano and McBride*, 1998].

Consistency among our records and other records located on the boundary of the ITCZ, including δ^{18}O of stalagmite in Cave of Oman [*Fleitmann et al*., 2003], Ti counts in the Cariaco Basin [*Haug et al*., 2001], δ^{18}O of fossil drip-water in Peru and insolation change at 30°N averaged from June to August [*Berger and Loutre*, 1991; *Van Breukelen et al*., 2008], supports the global wide ITCZ modulation on monsoon systems, most likely as part of atmospheric adjustment in response to orbital forcing [*Fleitmann et al*., 2003; *Haug et al*., 2001] (Figure 8). These records collectively document a southward migration of the ITCZ since the early Holocene. This is a response to summer insolation in the northern hemisphere which was subjected to orbital precession during the Holocene retreat of large boreal ice sheets [*Arbuszewski et al*., 2013].

In another words, the East Asian monsoon is likely controlled by both aforementioned internal and external forcing [*Wang*, 2009]. At the millennial scale, we also identity the antiphase phenomenon between the GSI and δ^{18}O of stalagmite in Dongge Cave, particularly during the Young Dryas and Bølling-Allerød (Figure 8); these periods are coincident with a change in ^{231}Pa/^{230}Th, a kinematic proxy for the Atlantic Meridional overturning circulation (AMOC) [*Gherardi et al*., 2005; *McManus et al*., 2004] (Figure 8). According to *Sun et al*. [2012], AMOC is the main driver of abrupt change in the East Asian winter and summer monsoon systems, and the westerly acts as a mediator in transmitting this signal from North Atlantic to the Asian monsoon regions. Furthermore, the average position of ITCZ is regulated by latitudinal gradients in sea surface temperature [*Chiang and Bitz*, 2005]. Therefore, the ITCZ migrates southward during cold periods in the North Atlantic when AMOC is reduced [*Broccoli et al*., 2006; *Schmidt and Spero*, 2011; *Stouffer et al*., 2006; *Vellinga and Wood*, 2002; *Vellinga and Wu*, 2004] and thus causes the millennial variations of the EAWM. This further implies that the high latitudes have an influence on EAWM at the millennial scale and thus supports the idea that the East Asian monsoon is controlled by both internal and external forcing at different time scales [*Wang*, 2009].

To unravel the effect of external forcing due to insolation and ENSO forcing, we ran a Cross-Correlation Analysis(CCA) for the East Asian winter and summer monsoon proxy using the free software 'R' [*Venables et al*., 2002] (Figure 10).The GSI and log(Ti/Ca) data were divided into three intervals from 12,000 cal yr BP to present according to the general variation in trend; specifically, the intervals are: 12,000–5500 cal yr BP, 5500–2500 cal yr BP and 2500–0 cal yr BP (Figures 8 and 10).

The GSI and log(Ti/Ca), when compared with δ^{18}O of stalagmite in Dongge Cave, have higher anticorrelated values of greater than −0.8 and show similar 2000, 1500 and 256 year cycles during 12,000–5500 cal yr BP period, indicating that the variation of the EAWM was controlled by broad-scale migration of the ITCZ (Figures 8 and 10). Recently, this result was confirmed by the existence of an inverse relationship between the East Asian winter and summer monsoon during the period 10,000–5500 cal yr BP, obtained from the new δ^{18}O stalagmite records of Itoigawa, Japan [*Sone et al*., 2013].

From 5500 to 2500 cal yr BP, the CCA value decreased to approximately −0.4 and −0.5, respectively, for the GSI and log(Ti/Ca) (Figure 10). The GSI lags the δ^{18}O of stalagmite in Dongge Cave by approximately 300 years. This lag might also be caused by uncertainty in the age model. On the other hand, the centennial cycle exhibited in the log(Ti/ca) and the δ^{18}O of Dongge stalagmite (256–512 years) are similar to the ENSO

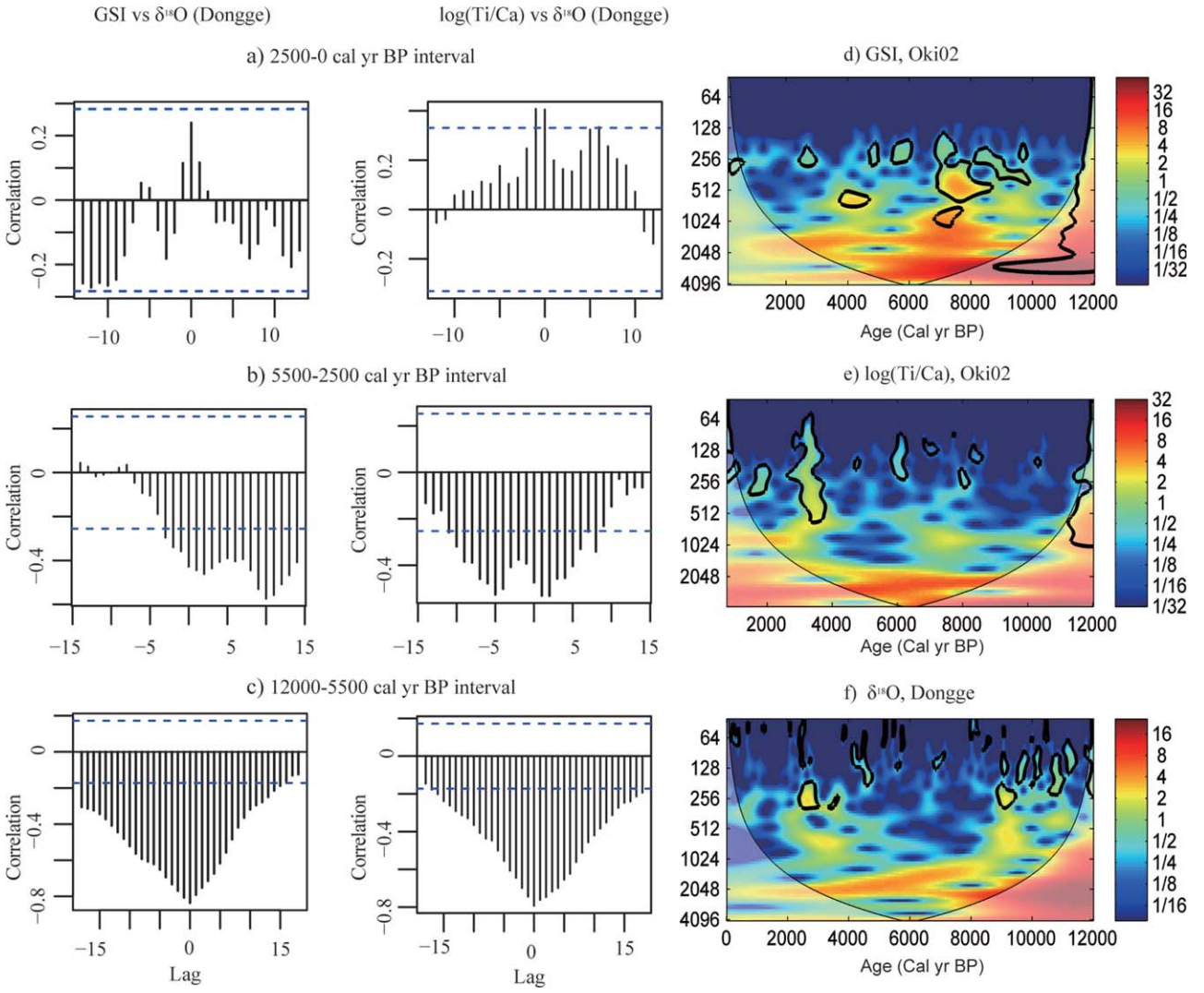

Figure 10. Cross-Correlation Analysis for (left) GSI and (right) log(Ti/Ca) against δ^{18}O of stalagmite in Dongge Cave for intervals of (a)12,000–5500 cal yr BP, (b) 5500–2500 cal yr BP, and (c) 2500–0 cal yr BP. Blue dash lines confine the 95% significance threshold, Wavelet analysis on (d) GSI, (e) log(Ti/Ca), and (f) δ^{18}O of stalagmites in Dongge, China, the black line indicates 99.98% confidence level for a red noise process.

cycles recorded in lake Laguna Pallcacocha and also significant periods of the δ^{14}C record [*Moy et al*., 2002] (Figure 10). The GSI and log(Ti/Ca) experienced significant increases likely associated with the southward migration of the ITCZ. In contrast, the decreasing CCA value during this period is ascribed to increase in ENSO activity (more *El Niño*) as mentioned previously in earlier studies. Recent modeling work proposes that anomalously warm temperatures in the equatorial Pacific Ocean, such as those occurring during an *El Niño* event, significantly alters the strength of the EASM by about 10% on average and 40% in individually strong events [*Bush*, 2001; *Wang et al*., 2003]. The warm/cold events in the eastern Pacific namely *El Niño/La Niña* events could also modify the EAWM via an anomalous lower tropospheric anticyclone located in the western North Pacific [*Wang et al*., 2000]. The intensified ENSO activity would act as an internal feedback possibly interfering with the monsoon's response to insolation which could decouple the EASM and EAWM.

On the other hand, the response time of the monsoons to insolation forcing or to ENSO may differ substantially between different regions due to distinct oceanic feedbacks [*Liu et al*., 2003] and the oceanic feedback may also lead to the inhomogeneous response of monsoons in the Holocene [*Liu et al*., 2003]. Recent meteorological observations also proved that different modes of tropical Pacific sea surface temperature could result in an out-of-phase of EASM on the interannual and precession scales [*Shi et al*., 2012]. Obviously, the

enhancement of ENSO may result in a decoupling or lagging between the East Asian winter and summer monsoon and, therefore, explain the CCA values (Figure 10).

In the most recent 2500 years, the CCA correlation value for log(Ti/Ca) shifted to positive, yet both the GSI and log(Ti/Ca) correlations are outside the range of our confidence (dashed line, $p>0.05$) (Figure 10). The centennial cycle was also identified in the GSI, log(Ti/Ca) and $\delta^{18}O$ of stalagmite for this period (Figure 10). The transition from negative to positive with a poor relationship among proxies suggests a weaker coupling relationship between the East Asian winter and summer monsoon. The further enhancement of ENSO since 3000 cal yr BP has been reported by modeling efforts and other proxies [*Donders et al*., 2008; *Loubere et al*., 2012; *Moy et al*., 2002; *Woodroffe et al*., 2003]. This interval relates to a much higher ENSO frequency than preceding period (5500–2500 cal yr BP), from initially less than 10 *El Niño* events to up to 31 *El Niño* events per century [*Marriner et al*., 2012; *Moy et al*., 2002]. Moreover, increased anthropogenic interference on the climate and environment has had a significant impact since 2500 cal yr BP [*Bayon et al*., 2012; *Ruddiman and Ellis*, 2009; *Ruddiman et al*., 2011]. The intensification of human land-use was proposed to have caused a major change in vegetation from rainforest trees to savannas, and an intensified weathering in Central Africa since 3000 cal yr BP [*Bayon et al*., 2012]. Greater forest clearance by early agriculturalists could also have had a disproportionately large impact on CO_2 emissions and the total forest clearance show faster rises prior to 2000 years ago followed by a leveling out [*Ruddiman and Ellis*, 2009]. Recent modeling results show that vegetation, soil moisture and CO_2 acting as internal feedbacks might alter the monsoon's response to external forcing [*Kutzbach et al*., 1996; *Wang et al*., 2005]. Thus, the intensified ENSO, coupled with a greater anthropogenic interference, since approximately 2500 cal yr BP, might have had a great impact on the climate system, thus causing the complexity and nonlinear relationship between the East Asian winter and summer monsoon.

5. Conclusion

High resolution sedimentary record retrieved from a deep sea fan in the Okinawa Trough allowed us to reconstruct the EAWM during the Holocene. Clay mineral analysis of bulk sediment shows that the material was derived primarily from mainland China, with minor amounts coming from Taiwan and the Yellow River since the Holocene. Sedimentation has been mainly controlled by the bottom nepheloid layer (33%) and the upper layers transport (33%) dominates in the EAWM, but it has been influenced less by fluvial sources due to the obstruction of the Kuroshio-induced current since the Holocene. From the comparison of the temporal trends in the newly proposed grain size index (GSI) and log(Ti/Ca) with stalagmite record in Dongge cave, we observed significant anticorrelation between the EAWM and the EASM in the Holocene, suggesting that the migration of ITCZ modulate the EAWM. The similarity in the behavior of our records with rainfall records in Peru, located in the southern hemisphere, as well as the inverse relationship seen with the Ti counts in the Cariaco Basin, the monsoon records in Oman and averaged insolation changes at 30°N from June to August, further support the theory of broad ITCZ modulation on monsoon systems globally. Cross-Correlation Analysis at different time intervals of grain size index (GSI) and log(Ti/Ca) against the $\delta^{18}O$ of stalagmites in Dongge Cave suggests a decoupling and lagging relationship between the East Asian winter and summer monsoon during 5500–2500 cal yr BP, and an even more complicated relationship during the period of 2500–0 cal yr BP which is attributable to enhanced ENSO activity and growing human interference.

Acknowledgments

Our work is supported by the National Natural Science Foundation of China (40776030, 41376057) and the Strategic Priority Research Program of the Chinese Academy of Sciences (XDA11030302). We thank Zhengquan Yao for XRF measurements and Hongli Wang for grain size measurement. We are grateful to Dennis Darby at Old Dominion University and anonymous reviewers for providing valuable advice on our manuscript.

References

An, Z. (2000), The history and variability of the East Asian paleomonsoon climate, *Quat. Sci. Rev.*, *19*(1–5), 171–187, doi:10.1016/S0277-3791(99)00060-8.

An, Z., L. Tunghseng, L. Yanchou, S. Porter, G. Kukla, W. Xihao, and H. Yingming (1990), The long-term paleomonsoon variation recorded by the loess-paleosol sequence in central China, *Quat. Int.*, *7*, 91–95, doi:10.1016/1040-6182(90)90042-3.

Arbuszewski, J. A., P. B. Demenocal, C. Cleroux, L. Bradtmiller, and A. Mix (2013), Meridional shifts of the Atlantic intertropical convergence zone since the Last Glacial Maximum, *Nat. Geosci.*, *6*, 959–962, doi:10.1038/ngeo1961.

Arz, H., J. Pätzold, and G. Wefer (1998), Correlated millennial-scale changes in surface hydrography and terrigenous sediment yield inferred from last-glacial marine deposits off northeastern Brazil, *Quat. Res.*, *50*, QR981992, 157–166, doi:10.1006/qres.1998.1992.

Arz, H., J. Pätzold, and G. Wefer (1999), Climatic changes during the last deglaciation recorded in sediment cores from the northeastern Brazilian Continental Margin, *Geo-Mar. Lett.*, *19*(3), 209–218, doi:10.1007/s003670050111.

Bayon, G., B. Dennielou, J. Etoubleau, E. Ponzevera, S. Toucanne, and S. Bermell (2012), Intensifying weathering and land use in Iron Age Central Africa, *Science*, *335*(6073), 1219–1222, doi:10.1126/science.1215400.

Berger, A., and M.-F. Loutre (1991), Insolation values for the climate of the last 10 million years, *Quat. Sci. Rev.*, *10*(4), 297–317, doi:10.1016/0277–3791(91)90033-Q.
Bian, C. W., W. S. Jiang, and D. H. Song (2010), Terrigenous transportation to the Okinawa Trough and the influence of typhoons on suspended sediment concentration, *Cont. Shelf Res.*, *30*(10–11), 1189–1199, doi:10.1016/j.csr.2010.03.008.
Biscaye, P. E. (1965), Mineralogy and sedimentation of recent deep-sea clay in the Atlantic Ocean and adjacent seas and oceans, *Geol. Soc. Am. Bull.*, *76*(7), 803–832.
Bouma, A. (2001), Fine-grained submarine fans as possible recorders of long-and short-term climatic changes, *Global Planet. Change*, *28*(1), 85–91, doi:10.1016/S0921–8181(00)00066-7.
Broccoli, A. J., K. A. Dahl, and R. J. Stouffer (2006), Response of the ITCZ to Northern Hemisphere cooling, *Geophys. Res. Lett.*, *33*, L01702, doi:10.1029/2005GL024546.
Bush, A. B. G. (2001), Pacific sea surface temperature forcing dominates orbital forcing of the early Holocene monsoon, *Quat. Res.*, *55*(1), 25–32, doi:10.1006/qres.2000.2198.
Chao, W. C., and B. Chen (2001), The origin of monsoons, *J. Atmos. Sci.*, *58*(22), 3497–3507, doi:10.1175/1520-0469(2001)058<3497:TOOM>2.0.CO;2.
Chiang, J. C., and C. M. Bitz (2005), Influence of high latitude ice cover on the marine Intertropical Convergence Zone, *Clim. Dyn.*, *25*(5), 477–496, doi:10.1007/s00382-005-0040-5.
Clark, P., A. Dyke, J. Shakun, A. Carlson, J. Clark, B. Wohlfarth, J. Mitrovica, S. Hostetler, and A. McCabe (2009), The Last Glacial Maximum, *Science*, *325*(5941), 710–714, doi:10.1126/science.1172873.
Clement, A. C., R. Seager, and M. A. Cane (2000), Suppression of El Niño during the Mid-Holocene by changes in the Earth's orbit, *Paleoceanography*, *15*(6), 731–737, doi:10.1029/1999PA000466.
Conroy, J. L., J. T. Overpeck, J. E. Cole, T. M. Shanahan, and M. Steinitz-Kannan (2008), Holocene changes in eastern tropical Pacific climate inferred from a Galápagos lake sediment record, *Quat. Sci. Rev.*, *27*(11), 1166–1180, doi:10.1016/j.quascirev.2008.02.015.
Darby, D. A., J. Ortiz, L. Polyak, S. Lund, M. Jakobsson, and R. A. Woodgate (2009), The role of currents and sea ice in both slowly deposited central Arctic and rapidly deposited Chukchi-Alaskan margin sediments, *Global Planet. Change*, *68*, 58–72, doi:10.1016/j.gloplacha.2009.02.007.
de Garidel-Thoron, T., L. Beaufort, B. K. Linsley, and S. Dannenmann (2001), Millennial-scale dynamics of the East Asian winter monsoon during the last 200,000 years, *Paleoceanography*, *16*(5), 491–502, doi:10.1029/2000PA000557.
Diekmann, B., J. Hofmann, R. Henrich, D. K. Fütterer, U. Röhl, and K.-Y. Wei (2008), Detrital sediment supply in the southern Okinawa Trough and its relation to sea-level and Kuroshio dynamics during the late Quaternary, *Mar. Geol.*, *255*(1), 83–95, doi:10.1016/j.margeo.2008.08.001.
Donders, T. H., F. Wagner-Cremer, and H. Visscher (2008), Integration of proxy data and model scenarios for the mid-Holocene onset of modern ENSO variability, *Quat. Sci. Rev.*, *27*(5), 571–579, doi:10.1016/j.quascirev.2007.11.010.
Dou, Y., S. Yang, Z. Liu, P. D. Clift, H. Yu, S. Berne, and X. Shi (2010), Clay mineral evolution in the central Okinawa Trough since 28ka: Implications for sediment provenance and paleoenvironmental change, *Palaeogeogr. Palaeoclimatol. Palaeoecol.*, *288*(1), 108–117, doi:j.palaeo.2010.01.040.
Dou, Y., S. Yang, M. Tang, Z. Liu, and H. Yu (2011), Using biogenic components to decipher the terrigenous input and paleoenvironmental changes over the last 28ka in the middle Okinawa Trough, *Quat. Sci.*, *31*(2), 236–243, doi:10.3969/j.issn.10017410.2011.02.0.
Dou, Y., S. Yang, Z. Liu, J. Li, X. Shi, H. Yu, and S. Berne (2012), Sr–Nd isotopic constraints on terrigenous sediment provenances and Kuroshio Current variability in the Okinawa Trough during the late Quaternary, *Palaeogeogr. Palaeoclimatol. Palaeoecol.*, *365*, 38–47, doi:10.1016/j.palaeo.2012.09.003.
Dyke, A. S., and V. K. Prest (1987), Late Wisconsinan and Holocene history of the Laurentide ice sheet, *Geogr. Phys. Quat.*, *41*(2), 237–263.
Dykoski, C. A., R. L. Edwards, H. Cheng, D. Yuan, Y. Cai, M. Zhang, Y. Lin, J. Qing, Z. An, and J. Revenaugh (2005), A high-resolution, absolute-dated Holocene and deglacial Asian monsoon record from Dongge Cave, China, *Earth Planet. Sci. Lett.*, *233*(1), 71–86, doi:10.1016/j.epsl.2005.01.036.
Fleitmann, D., S. J. Burns, M. Mudelsee, U. Neff, J. Kramers, A. Mangini, and A. Matter (2003), Holocene forcing of the Indian monsoon recorded in a stalagmite from southern Oman, *Science*, *300*(5626), 1737–1739, doi:10.1126/science.1083130.
Gadgil, S. (2003), The Indian monsoon and its variability, *Annu. Rev. Earth Planet. Sci.*, *31*(1), 429–467, doi:10.1016/j.epsl.2005.09.061.
Gherardi, J.-M., L. Labeyrie, J. McManus, R. Francois, L. Skinner, and E. Cortijo (2005), Evidence from the Northeastern Atlantic basin for variability in the rate of the meridional overturning circulation through the last deglaciation, *Earth Planet. Sci. Lett.*, *240*(3), 710–723, doi:10.1016/j.epsl.2005.09.061.
Hajian, S., and M. S. Movahed (2010), Multifractal detrended cross-correlation analysis of sunspot numbers and river flow fluctuations, *Physica A*, *389*(21), 4942–4957, doi:10.1016/j.physa.2010.06.025.
Haug, G. H., K. A. Hughen, D. M. Sigman, L. C. Peterson, and U. Röhl (2001), Southward migration of the Intertropical Convergence Zone through the Holocene, *Science*, *293*(5533), 1304–1308, doi:10.1126/science.1059725.
Hoshika, A., T. Tanimoto, Y. Mishima, K. Iseki, and K. Okamura (2003), Variation of turbidity and particle transport in the bottom layer of the East China Sea, *Deep Sea Res., Part II*, *50*, 443–455, doi:10.1016/S0967-0645(02)00462-9.
Hsu, S. C., S.-J. Kao, and W.-L. Jeng (2006), Quantitative links between fluvial sediment discharge, trapped terrigenous flux and sediment accumulation, and implications for temporal and spatial distributions of sediment fluxes, *Deep Sea Res., Part I*, *53*(2), 241–252, doi:10.1016/j.dsr.2005.10.001.
Hsu, S. C., S. C. Liu, R. Arimoto, T. H. Liu, Y. T. Huang, F. Tsai, F. J. Lin, and S. J. Kao (2009), Dust deposition to the East China Sea and its biogeochemical implications, *J. Geophys. Res.*, *114*, D15304, doi:10.1029/2008JD011223.
Hsu, T. J., and D. M. Hanes (2004), Effects of wave shape on sheet flow sediment transport, *J. Geophys. Res.*, *109*, C05025, doi:10.1029/2003JC002075.
Huh, C. A., C.-C. Su, W.-T. Liang, and C.-Y. Ling (2004), Linkages between turbidites in the southern Okinawa Trough and submarine earthquakes, *Geophys. Res. Lett.*, *31*, L12304, doi:10.1029/2004GL019731.
Iseki, K., K. Okamura, and Y. Kiyomoto (2003), Seasonality and composition of downward particulate fluxes at the continental shelf and Okinawa Trough in the East China Sea, *Deep Sea Res., Part II*, *50*(2), 457–473, doi:10.1016/S0967-0645(02)00468-X.
Kagimoto, T., and T. Yamagata (1997), Seasonal transport variations of the Kuroshio: An OGCM simulation, *J. Phys. Oceanogr.*, *27*(3), 403–418, doi:10.1175/1520-0485(1997)027<0403:STVOTK>2.0.CO;2.
Kao, S. J., C.-R. Wu, Y.C. Hsin, and M. Dai (2006), Effects of sea level change on the upstream Kuroshio Current through the Okinawa Trough. *Geophys. Res. Lett.*, *33*, L16604, doi:10.1029/2006GL026822.
Kao, S. J., J. Sen, S. C. Hsu, T. Y. Lee, and M. Dai (2008a), Sediment budget in the Taiwan Strait with high fluvial sediment inputs from mountainous rivers: New observations and synthesis, *Terrestrial Atmos. Ocean Sci.*, *19*, 525–546, doi:10.3319/TAO.2008.19.5.525(Oc).

Kao, S. J., M. H. Dai, K. Y. Wei, N. E. Blair, and W. B. Lyons (2008b), Enhanced supply of fossil organic carbon to the Okinawa Trough since the last deglaciation, *Paleoceanography*, *23*, PA2207, doi:10.1029/2007PA001440.
Kineke, G., K. Woolfe, S. Kuehl, J. Milliman, T. Dellapenna, and R. Purdon (2000), Sediment export from the Sepik River, Papua New Guinea: Evidence for a divergent sediment plume, *Cont. Shelf Res.*, *20*(16), 2239–2266, doi:10.1016/S0278-4343(00)00069-8.
Kutzbach, J., G. Bonan, J. Foley, and S. P. Harrison (1996), Vegetation and soil feedbacks on the response of the African monsoon to orbital forcing in the early to middle Holocene, *Nature*, *384*, 623–626, doi:10.1038/384623a0.
Kutzbach, J., R. Gallimore, S. Harrison, P. Behling, R. Selin, and F. Laarif (1998), Climate and biome simulations for the past 21,000 years, *Quat. Sci. Rev.*, *17*, 473–506, doi:10.1016/S0277-3791(98)00009-2.
Lambeck, K., and J. Chappell (2001), Sea level change through the last glacial cycle, *Science*, *292*(5517), 679–686, doi:10.1126/science.1059549.
Lee, H.-J., and S.-Y. Chao (2003), A climatological description of circulation in and around the East China Sea, *Deep Sea Res., Part II*, *50*(6), 1065–1084, doi:10.1016/S0967-0645(03)00010-9.
Lee, K. E., H. J. Lee, J. H. Park, Y. P. Chang, K. Ikehara, T. Itaki, and H. K. Kwon (2013), Stability of the Kuroshio path with respect to glacial sea level lowering, *Geophys. Res. Lett.*, *40*, 392–396, doi:10.1012/grl.50102.
Li, C., X. Shi, S. Kao, M. Chen, Y. Liu, X. Fang, H. Lü, J. Zou, S. Liu, and S. Qiao (2012), Clay mineral composition and their sources for the fluvial sediments of Taiwanese rivers, *Chin. Sci. Bull.*, *57*(6), 673–681, doi:10.1007/s11434-011-4824-1.
Li, T., Z. Liu, M. A. Hall, S. Berne, Y. Saito, S. Cang, and Z. Cheng (2001), Heinrich event imprints in the Okinawa Trough: Evidence from oxygen isotope and planktonic foraminifera, *Palaeogeogr. Palaeoclimatol. Palaeoecol.*, *176*(1), 133–146, doi:10.1016/S0031–0182(01)00332-7.
Li, Y. H. (1976), Denudation of Taiwan island since the Pliocene epoch, *Geology*, *4*(2), 105–107.
Liu, J., C. Liu, K. Xu, J. Milliman, J. Chiu, S. Kao, and S. Lin (2008), Flux and fate of small mountainous rivers derived sediments into the Taiwan Strait, *Mar. Geol.*, *256*(1), 65–76, doi:10.1016/j.margeo.2008.09.007.
Liu, J. P., J. D. Milliman, S. Gao, and P. Cheng (2004), Holocene development of the Yellow River's subaqueous delta, North Yellow Sea, *Mar. Geol.*, *209*(1), 45–67, doi:10.1016/j.margeo.2004.06.009.
Liu, J. T., S.-J. Kao, C.-A. Huh, and C.-C. Hung (2013), Gravity flows associated with flood events and carbon burial: Taiwan as instructional source area, *Annu. Rev. Mar. Sci.*, *5*, 47–68, doi:10.1146/annurev-marine-121211-172307.
Liu, X., H. Dong, X. Yang, U. Herzschuh, E. Zhang, J.-B. W. Stuut, and Y. Wang (2009), Late Holocene forcing of the Asian winter and summer monsoon as evidenced by proxy records from the northern Qinghai–Tibetan Plateau, *Earth Planet. Sci. Lett.*, *280*(1), 276–284, doi:10.1016/j.epsl.2009.01.041.
Liu, Z., J. Kutzbach, and L. Wu (2000), Modeling climate shift of El Niño variability in the Holocene, *Geophys. Res. Lett.*, *27*(15), 2265–2268, doi:10.1029/2000GL011452.
Liu, Z., B. Otto-Bliesner, J. Kutzbach, L. Li, and C. Shields (2003), Coupled climate simulation of the evolution of global monsoons in the Holocene, *J. Clim.*, *16*, 2472–2490, doi:10.1175/1520-0442(2003)016<2472:CCSOTE>2.0.CO;2.
Loubere, P., W. Creamer, and J. Haas (2012), Evolution of the El Nino-Southern Oscillation in the late Holocene and insolation driven change in the tropical annual SST cycle, *Global Planet. Change*, *100*, 129–144, doi:10.1016/j.gloplacha.2012.10.007.
Machida, H. (1999), The stratigraphy, chronology and distribution of distal marker-tephras in and around Japan, *Global Planet. Change*, *21*(1), 71–94, doi:10.1016/S0921–8181(99)00008–9.
Maher, B. A., and M. Hu (2006), A high-resolution record of Holocene rainfall variations from the western Chinese Loess Plateau: Antiphase behaviour of the African/Indian and East Asian summer monsoons, *Holocene*, *16*(3), 309–319, doi:10.1191/0959683606hl929rp.
Marriner, N., C. Flaux, D. Kaniewski, C. Morhange, G. Leduc, V. Moron, Z. Chen, F. Gasse, J.-Y. Empereur, and J.-D. Stanley (2012), ITCZ and ENSO-like pacing of Nile delta hydro-geomorphology during the Holocene, *Quat. Sci. Rev.*, *45*, 73–84, doi:10.1016/j.quascirev.2012.04.022.
McCave, I., B. Manighetti, and S. Robinson (1995), Sortable silt and fine sediment size/composition slicing: Parameters for palaeocurrent speed and palaeoceanography, *Paleoceanography*, *10*(3), 593–610, doi:10.1029/94PA03039.
McManus, J., R. Francois, J.-M. Gherardi, L. Keigwin, and S. Brown-Leger (2004), Collapse and rapid resumption of Atlantic meridional circulation linked to deglacial climate changes, *Nature*, *428*(6985), 834–837, doi:10.1038/nature02494.
Milliman, J. D., and R. H. Meade (1983), World-wide delivery of river sediment to the oceans, *J. Geol.*, *91*, 1–21.
Milliman, J. D., and J. D. M. Syvitski (1992), Geomorphic/tectonic control of sediment discharge to the ocean: The importance of small mountainous rivers, *J. Geol.*, *100*, 525–544.
Moy, C. M., G. O. Seltzer, D. T. Rodbell, and D. M. Anderson (2002), Variability of El Niño/Southern Oscillation activity at millennial timescales during the Holocene epoch, *Nature*, *420*(6912), 162–165. doi:10.1038/nature01194.
Nagashima, K., R. Tada, H. Matsui, T. Irino, A. Tani, and S. Toyoda (2007), Orbital-and millennial-scale variations in Asian dust transport path to the Japan Sea, *Palaeogeogr. Palaeoclimatol. Palaeoecol.*, *247*(1), 144–161, doi:10.1016/j.palaeo.2006.11.027.
Oguri, K., E. Matsumoto, Y. Saito, M. C. Honda, N. Harada, and M. Kusakabe (2000), Evidence of the offshore transport of terrestrial organic matter due to the rise of sea level: The case of the East China Sea continental shelf, *Geophys. Res. Lett.*, *27*(23), 3893–3896, doi:10.1029/2000GL011690.
Oguri, K., E. Matsumoto, M. Yamada, Y. Saito, and K. Iseki (2003), Sediment accumulation rates and budgets of depositing particles of the East China Sea, *Deep Sea Res., Part II*, *50*(2), 513–528, doi:10.1016/S0967-0645(02)00465-4.
Qu, T., and R. Lukas (2003), The bifurcation of the North Equatorial Current in the Pacific, *J. Phys. Oceanogr.*, *33*(1), 5–18, doi:10.1175/1520-0485(2003)033<0005:TBOTNE>2.0.CO;2.
Qu, T., Y. Y. Kim, M. Yaremchuk, T. Tozuka, A. Ishida, and T. Yamagata (2004), Can Luzon Strait transport play a role in conveying the impact of ENSO to the South China Sea?, *J. Clim.*, *17*, 3644–3657, doi:10.1175/1520-0442(2004)017<3644:CLSTPA>2.0.CO;2.
Rodbell, D. T., G. O. Seltzer, D. M. Anderson, M. B. Abbott, D. B. Enfield, and J. H. Newman (1999), An∼ 15,000-year record of El Niño-driven alluviation in southwestern Ecuador, *Science*, *283*(5401), 516–520, doi:10.1126/science.283.5401.516.
Ruddiman, W. F., and E. C. Ellis (2009), Effect of per-capita land use changes on Holocene forest clearance and CO2 emissions, *Quat. Sci. Rev.*, *28*(27), 3011–3015, doi:10.1016/j.quascirev.2009.05.022.
Ruddiman, W. F., J. E. Kutzbach, and S. J. Vavrus (2011), Can natural or anthropogenic explanations of late-Holocene CO_2 and CH_4 increases be falsified?, *Holocene*, *21*(5), 865–879, doi:10.1177/0959683610387172.
Saito, Y., H. Katayama, K. Ikehara, Y. Kato, E. Matsumoto, K. Oguri, M. Oda, and M. Yumoto (1998), Transgressive and highstand systems tracts and post-glacial transgression, the East China Sea, *Sediment. Geol.*, *122*(1), 217–232, doi:10.1016/S0037-0738(98)00107-9.
Schmidt, M. W., and H. J. Spero (2011), Meridional shifts in the marine ITCZ and the tropical hydrologic cycle over the last three glacial cycles, *Paleoceanography*, *26*, PA1206, doi:10.1029/2010PA001976.

Shi, Z., X. Liu, and X. Cheng (2012), Anti-phased response of northern and southern East Asian summer precipitation to ENSO modulation of orbital forcing, *Quat. Sci. Rev.*, *40*, 30–38, doi:10.1016/j.quascirev.2012.02.019.
Sone, T., A. Kano, T. Okumura, K. Kashiwagi, M. Hori, X. Jiang, and C.-C. Shen (2013), Holocene stalagmite oxygen isotopic record from the Japan Sea side of the Japanese Islands, as a new proxy of the East Asian winter monsoon, *Quat. Sci. Rev.*, *75*, 150–160, doi:10.1016/j.quascirev.2013.06.019.
Steinke, S., T. J. Hanebuth, C. Vogt, and K. Stattegger (2008), Sea level induced variations in clay mineral composition in the southwestern South China Sea over the past 17,000 yrs, *Mar. Geol.*, *250*(3), 199–210, doi:10.1016/j.margeo.2008.01.005.
Steinke, S., C. Glatz, M. Mohtadi, J. Groeneveld, Q. Li, and Z. Jian (2011), Past dynamics of the East Asian monsoon: No inverse behaviour between the summer and winter monsoon during the Holocene, *Global Planet. Change*, *78*(3), 170–177, doi:10.1016/j.gloplacha.2011.06.006.
Stouffer, R. J., J. Yin, J. Gregory, K. Dixon, M. Spelman, W. Hurlin, A. Weaver, M. Eby, G. Flato, and H. Hasumi (2006), Investigating the causes of the response of the thermohaline circulation to past and future climate changes, *J. Clim.*, *19*, 1365–1387. doi:10.1175/JCLI3689.1.
Sun, Y., S. Gao, and J. Li (2003), Preliminary analysis of grain-size populations with environmentally sensitive terrigenous components in marginal sea setting, *Chin. Sci. Bull.*, *48*(2), 184–187, doi:10.1360/03tb9038.
Sun, Y., D. W. Oppo, R. Xiang, W. Liu, and S. Gao (2005), Last deglaciation in the Okinawa Trough: Subtropical northwest Pacific link to Northern Hemisphere and tropical climate, *Paleoceanography*, *20*, PA4005, doi:10.1029/2004PA001061.
Sun, Y., S. C. Clemens, C. Morrill, X. Lin, X. Wang, and Z. An (2012), Influence of Atlantic meridional overturning circulation on the East Asian winter monsoon, *Nat. Geosci.*, *5*(1), 46–49, doi:10.1038/NGEO1326.
Tian, J., E. Huang, and D. K. Pak (2010), East Asian winter monsoon variability over the last glacial cycle: Insights from a latitudinal sea-surface temperature gradient across the South China Sea, *Palaeogeogr. Palaeoclimatol. Palaeoecol.*, *292*(1), 319–324, doi:10.1016/j.palaeo.2010.04.005.
Torrence, C., and G. P. Compo (1998), A practical guide to wavelet analysis, *Bull. Am. Meteorol. Soc.*, *79*(1), 61–78, doi:10.1175/1520-0477(1998)079<0061:APGTWA>2.0.CO;2.
Tudhope, A. W., C. P. Chilcott, M. T. McCulloch, E. R. Cook, J. Chappell, R. M. Ellam, D. W. Lea, J. M. Lough, and G. B. Shimmield (2001), Variability in the El Niño-Southern Oscillation through a glacial-interglacial cycle, *Science*, *291*(5508), 1511–1517, doi:10.1126/science.1057969.
Van Breukelen, M., H. Vonhof, J. Hellstrom, W. Wester, and D. Kroon (2008), Fossil dripwater in stalagmites reveals Holocene temperature and rainfall variation in Amazonia, *Earth Planet. Sci. Lett.*, *275*(1), 54–60, doi:10.1016/j.epsl.2008.07.060.
Vellinga, M., and R. A. Wood (2002), Global climatic impacts of a collapse of the Atlantic thermohaline circulation, *Clim. Change*, *54*(3), 251–267, doi:10.1023/A:1016168827653.
Vellinga, M., and P. Wu (2004), Low-latitude freshwater influence on centennial variability of the Atlantic thermohaline circulation, *J. Clim.*, *17*(23), doi:10.1175/3219.1.
Venables, W., D. Smith, and the R Development Core Team (2002), *An Introduction to R, 2(1)*, pp. 1–90, Network Theory Ltd., Bristol, U. K.
Wan, S., A. Li, P. D. Clift, and J.-B. W. Stuut (2007), Development of the East Asian monsoon: Mineralogical and sedimentologic records in the northern South China Sea since 20 Ma, *Palaeogeogr. Palaeoclimatol. Palaeoecol.*, *254*(3), 561–582, doi:10.1016/j.palaeo.2007.07.009.
Wan, S., J. Tian, S. Steinke, A. Li, and T. Li (2010), Evolution and variability of the East Asian summer monsoon during the Pliocene: Evidence from clay mineral records of the South China Sea, *Palaeogeogr. Palaeoclimatol. Palaeoecol.*, *293*(1), 237–247, doi:10.1016/j.palaeo.2010.05.025.
Wan, S., Z. Yu, P. D. Clift, H. Sun, A. Li, and T. Li (2012), History of Asian eolian input to the West Philippine Sea over the last one million years, *Palaeogeogr. Palaeoclimatol. Palaeoecol.*, *326*, 152–159, doi:10.1016/j.palaeo.2012.02.015.
Wang, B., R. Wu, and X. Fu (2000), Pacific-East Asian teleconnection: How does ENSO affect East Asian climate?, *J. Clim.*, *13*(9), 1517–1536, doi:10.1175/1520-0442(2000)013<1517:PEATHD>2.0.CO;2.
Wang, B., S. C. Clemens, and P. Liu (2003), Contrasting the Indian and East Asian monsoons: Implications on geologic timescales, *Mar. Geol.*, *201*(1), 5–21, doi:10.1016/S0025–3227(03)00196-8.
Wang, J., A. Li, and J. Huang (2013), Sediment provenance and paleoenvironment records of the central Okinawa Trough for the 17000 years [in Chinese with English abstract], *Mar. Geol. Quat. Geol.*, *33*(6), 105–114, doi:10.3724/SpJ.1140.2013.06105.
Wang, L., J. Li, H. Lu, Z. Gu, P. Rioual, Q. Hao, A. W. Mackay, W. Jiang, B. Cai, and B. Xu (2012), The East Asian winter monsoon over the last 15,000 years: Its links to high-latitudes and tropical climate systems and complex correlation to the summer monsoon, *Quat. Sci. Rev.*, *32*, 131–142, doi:10.1016/j.quascirev.2011.11.003.
Wang, P. (2009), Global monsoon in a geological perspective, *Chin. Sci. Bull.*, *54*(7), 1113–1136, doi:10.1007/s11434-009-0169-4.
Wang, P., S. Clemens, L. Beaufort, P. Braconnot, G. Ganssen, Z. Jian, P. Kershaw, and M. Sarnthein (2005), Evolution and variability of the Asian monsoon system: State of the art and outstanding issues, *Quat. Sci. Rev.*, *24*(5), 595–629, doi:10.1016/j.quascirev.2004.10.002.
Wanner, H., J. Beer, J. Bütikofer, T. J. Crowley, U. Cubasch, J. Flückiger, H. Goosse, M. Grosjean, F. Joos, and J. O. Kaplan (2008), Mid-to Late Holocene climate change: An overview, *Quat. Sci. Rev.*, *27*(19), 1791–1828, doi:10.1016/j.quascirev.2008.06.013.
Wellner, R. W., and L. R. Bartek (2003), The effect of sea level, climate, and shelf physiography on the development of incised-valley complexes: A modern example from the East China Sea, *J. Sediment. Res.*, *73*(6), 926–940, doi:10.1306/041603730926.
Weltje, G. J., and R. Tjallingii (2008), Calibration of XRF core scanners for quantitative geochemical logging of sediment cores: Theory and application, *Earth Planet. Sci. Lett.*, *274*(3), 423–438, doi:10.1016/j.epsl.2008.07.054.
Woodroffe, C. D., M. R. Beech, and M. K. Gagan (2003), Mid-late Holocene El Niño variability in the equatorial Pacific from coral microatolls, *Geophys. Res. Lett.*, *30*(7), 1358, doi:10.1029/2002GL015868.
Xiang, R., Y. Sun, T. Li, D. W. Oppo, M. Chen, and F. Zheng (2007), Paleoenvironmental change in the middle Okinawa Trough since the last deglaciation: Evidence from the sedimentation rate and planktonic foraminiferal record, *Palaeogeogr. Palaeoclimatol. Palaeoecol.*, *243*(3), 378–393, doi:10.1016/j.palaeo.2006.
Xiao, J., S. C. Porter, Z. An, H. Kumai, and S. Yoshikawa (1995), Grain size of quartz as an indicator of winter monsoon strength on the Loess Plateau of central China during the last 130,000 yr, *Quat. Res.*, *43*(1), 22–29, doi:10.1006/qres.1995.1003.
Xiao, J., Y. Inouchi, H. Kumai, S. Yoshikawa, Y. Kondo, T. Liu, and Z. An (1997), Eolian quartz flux to Lake Biwa, central Japan, over the past 145,000 years, *Quat. Res.*, *48*(1), 48–57, doi:10.1006/qres.1997.1893.
Xiao, S., A. Li, J. P. Liu, M. Chen, Q. Xie, F. Jiang, T. Li, R. Xiang, and Z. Chen (2006), Coherence between solar activity and the East Asian winter monsoon variability in the past 8000 years from Yangtze River-derived mud in the East China Sea, *Palaeogeogr. Palaeoclimatol. Palaeoecol.*, *237*(2), 293–304, doi:10.1016/j.palaeo.2005.12.003.
Xu, K., J. D. Milliman, A. Li, J. Paul Liu, S.-J. Kao, and S. Wan (2009), Yangtze-and Taiwan-derived sediments on the inner shelf of East China Sea, *Cont. Shelf Res.*, *29*(18), 2240–2256, doi:10.1016/j.csr.2009.08.017.

Xu, K., A. Li, J. P. Liu, J. D. Milliman, Z. Yang, C. Liu, S. Kao, S. Wan, and F. Xu (2012), Provenance, structure, and formation of the mud wedge along inner continental shelf of the East China Sea: A synthesis of the Yangtze dispersal system, *Mar. Geol.*, *291–294*, 176–191, doi: 10.1016/j.margeo.2011.06.003.

Xu, X., and M. Oda (1999), Surface-water evolution of the eastern East China Sea during the last 36,000 years, *Mar. Geol.*, *156*, 285–304, doi: 10.1016/S0025-3227(98)00183-2.

Yanagi, T., S. Takahashi, A. Hoshika, and T. Tanimoto (1996), Seasonal variation in the transport of suspended matter in the East China Sea, *J. Oceanogr.*, *52*(5), 539–552,doi:10.1007/BF02238320.

Yancheva, G., N. R. Nowaczyk, J. Mingram, P. Dulski, G. Schettler, J. F. Negendank, J. Liu, D. M. Sigman, L. C. Peterson, and G. H. Haug (2007), Influence of the intertropical convergence zone on the East Asian monsoon, *Nature*, *445*(7123), 74–77, doi:10.1038/nature05431.

Yang, S. Y., H. S. Jung, D. I. Lim, and C. X. Li (2003), A review on the provenance discrimination of sediments in the Yellow Sea, *Earth Sci. Rev.*, *63*(1), 93–120, doi:10.1016/S0012-8252(03)00033-3.

Yang, Z., Z. Guo, Z. Wang, J. Xu, and W. Gao (1992), Basic pattern of transport of suspended matter from the Yellow Sea and East China Sea to the eastern deep seas, *Acta Oceanolog. Sin.*, *14*(2), 81–90.

Yano, J. I., and J. L. McBride (1998), An aquaplanet monsoon, *J. Atmos. Sci.*, *55*(8), 1373–1399, doi:10.1175/1520-0469(1998)055<1373:AAM>2.0.CO;2.

Yi, L., H.-J. Yu, J. D. Ortiz, X.-Y. Xu, S.-L. Chen, J.-Y. Ge, Q.-Z. Hao, J. Yao, X.-F. Shi, and S.-Z. Peng (2012), Late Quaternary linkage of sedimentary records to three astronomical rhythms and the Asian monsoon, inferred from a coastal borehole in the south Bohai Sea, China, *Palaeogeogr. Palaeoclimatol. Palaeoecol.*, *329*, 101–117, doi:10.1016/j.palaeo.2012.02.020.

Yoneda, M., H. Uno, Y. Shibata, R. Suzuki, Y. Kumamoto, K. Yoshida, T. Sasaki, A. Suzuki, and H. Kawahata (2007), Radiocarbon marine reservoir ages in the western Pacific estimated by pre-bomb molluscan shells, *Nucl. Instrum. Methods Phys.*, *259*(1), 432–437, doi:10.1016/j.nimb.2007.01.184.

Yuan, D., and Y. Hsueh (2010), Dynamics of the cross-shelf circulation in the Yellow and East China Seas in winter, *Deep Sea Res., Part II*, *57*(19), 1745–1761, doi:10.1016/j.dsr2.2010.04.002.

Yuan, D., J. Zhu, C. Li, and D. Hu (2008), Cross-shelf circulation in the Yellow and East China Seas indicated by MODIS satellite observations, *J. Mar. Syst.*, *70*(1), 134–149, doi:10.1016/j.jmarsys.2007.04.002.

Zhao, Y., B. H. Liu, S. X. Li, A. J. Cui, G. Z. Han, Q. F. Hua, and G. H. Hu (2011), Sedimentary characters and material transportation of submarine canyon-fan systems in slope of the East China Sea [in Chinese with English abstract], *J. Paleogeogr.*, *13*(1), 8.

Zhou, B., and P. Zhao (2009), Inverse correlation between ancient winter and summer monsoons in East Asia?, *Chin. Sci. Bull.*, *54*(20), 3760–3767, doi:10.1007/s11434-009-0583-7.